PHYSIK-DEPARTMENT

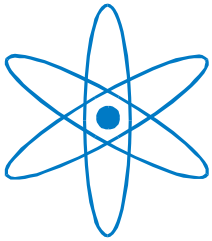

Search for Superheavy Elements in Nature with Accelerator Mass Spectrometry

Diploma Thesis
by

Peter Ludwig

TECHNISCHE UNIVERSITÄT
MÜNCHEN

Summary

For several decades, there have been predictions of an *island of stability* located around closed proton and neutron shells in the region N=184 and $108 \leq Z \leq 126$. If the half-lives of these superheavy elements (SHE) are long enough (on the order of 10^9 years), they could still exist in nature.

Accelerator Mass Spectrometry (AMS) is a powerful tool for the search for SHE in nature. Within the framework of this thesis, an existing AMS beamline at the Maier-Leibnitz-Laboratory in Garching was dismantled, rebuilt and equipped with a new Wien-filter for background reduction. The beamline's detection system features a time of flight spectrometer and an ionization chamber for energy and energy loss detection. It is especially suited for heavy isotope identification.

The masses A=292, 293, 294, 295, 298 and 310 were scanned for SHE in different sample materials, most importantly raw platinum, a promising material which has undergone a minimum of chemical processing and contains several possible chemical homologues for SHE. No events that could be attributed to SHE were recorded, which allowed us to set upper limits on the abundances of several SHE on the order of 10^{-14}-10^{-16} g/g in the sample materials.

A further implication of this work concerns the search for strange matter in nature. It is not excluded, that stable, atom-like strangelets are present on earth. It will be shown that the setup is also suited for searching for these strangelets.

Contents

1 Superheavy Elements

Superheavy Elements (SHE) are chemical elements with atomic numbers starting from Z=104 (rutherfordium). This thesis is based on the search for SHE in nature. For SHE to exist in nature, two main requirements must be fulfilled: A mechanism for the synthesis of SHE is needed and their half-life must be sufficiently long for them to have survived from the time of their synthesis until today.
This chapter gives an overview on the topic of superheavy elements. Their possible synthesis in nature, theoretical predictions on their stability, and different experimental approaches for their synthesis and search in nature will be discussed. An artist's impression of the search for the island of stability can be seen in figure 1.1.

1.1 Synthesis of the elements

One of the main goals of nuclear astrophysics is to understand the solar abundance distribution that can be observed in our sun's photosphere and in meteorites, see figure 1.2. In this section, an overview on nucleosynthesis is provided, with special focus on the rapid neutron capture process (r-process) which could be able to synthesize superheavy nuclei.

The earliest synthesis of elements heavier than hydrogen happened only minutes after the bing bang, when density and temperature were high enough to fuse hydrogen and neutrons to helium. However, these conditions were unable to synthesize elements heavier than lithium due to the extreme entropy ($\propto T^3/\rho$ in radiation-dominated matter) at that stage of development of the universe. Most of the other elements we can observe today are synthesized in stars.

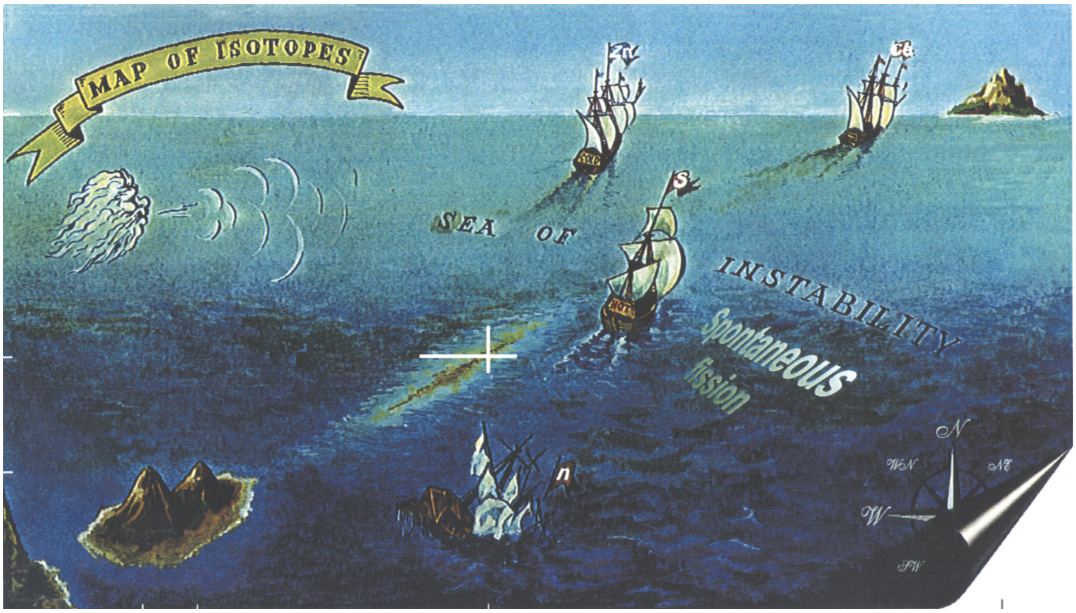

Figure 1.1: Artists impression of the search for the island of stability. The ships symbolize the various experimental techniques used the synthesis of superheavy elements, heading from the stable mountains in the south-west towards the island of stability in the north-east. Image by Yuri Oganessian.

1.1.1 Nuclear burning in stars

Hydrogen burning

Stars like our sun must produce energy to establish a hydrostatic equilibrium and avoid gravitational collapse. This energy is produced in nuclear fusion reactions.
Since hydrogen is the most abundant element in the universe, it is sensible to consider the collision of two protons as the first nuclear reaction towards energy generation in stars: $p(p, e^+\nu_e)d$. This reaction is the beginning of the pp-chain - the dominant chain of nuclear reactions that provides energy for stars with a relatively low temperature like our sun (below ∼20 MK for solar abundance distribution). Stars with higher temperature produce their energy dominantly in the CNO-cycles. Carbon, nitrogen, oxygen, and fluorine serve as catalysts for hydrogen burning.
The net reaction of the pp-chain and the CNO-chains is the same, they convert hydrogen into helium: $4\mathrm{H} \rightarrow {}^4\mathrm{He} + 2\mathrm{e}^+ + 2\nu_e$.

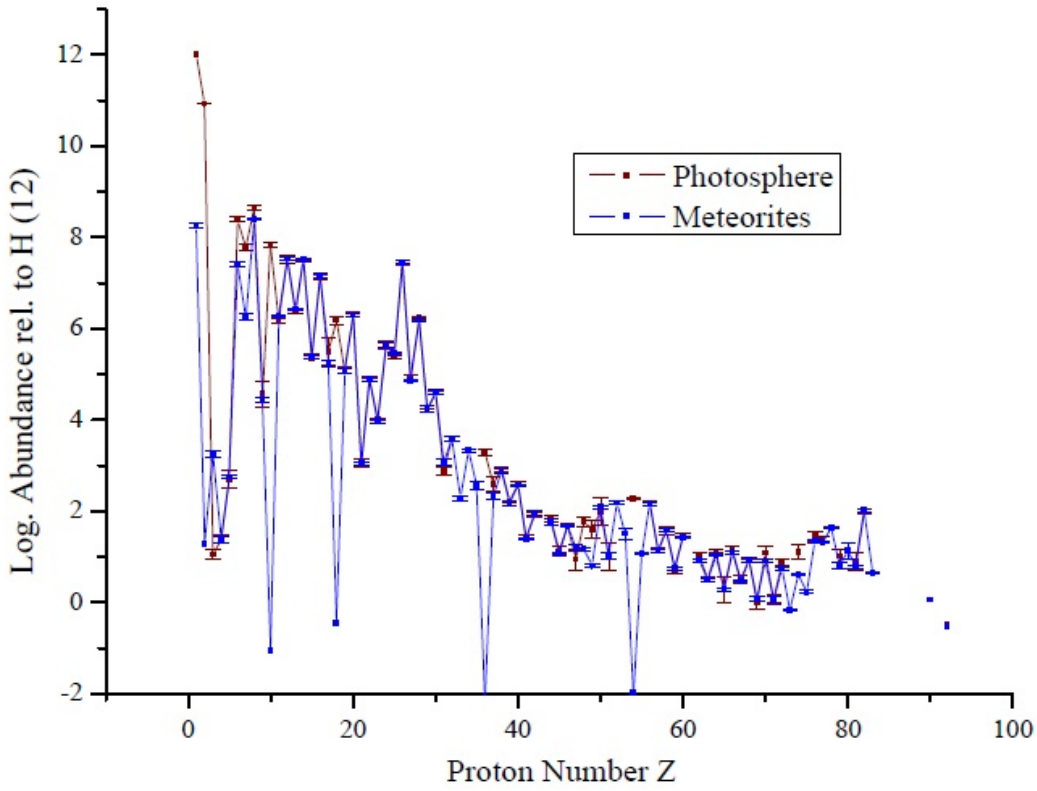

Figure 1.2: The figure shows the abundances of chemical elements in the solar photosphere and in meteorites [1]. We see an overall decrease in the elemental abundance with the proton number Z. Additionally, an even-odd effect is visible with higher abundances for nuclei with even Z and the closed proton shells Z=50,82 can be recognized by the relatively high abundances in those regions.

Advanced burning stages

After the hydrogen fuel in the core is exhausted, stars with $M > 0.4 \cdot M_{\odot}$ can start burning helium to carbon in the triple-alpha process. The extremely high temperature and density in even more massive stars ($M > 11 \cdot M_{\odot}$) lead to other successive burning stages: neon burning, oxygen burning, and silicon burning. After the fuel for one burning stage is exhausted in the center, it continues in a shell around the core, creating an onion-

like structure with a different burning stage in every shell.
The heaviest elements synthesized in this manner are in the iron region. The binding energy per nucleon is highest there, so heavier nuclei cannot be created in exothermic nuclear fusion reactions. To explain the observed elemental abundances (as seen in figure 1.2) in the solar system we need other processes to account for elements heavier than iron.

1.1.2 Nucleosynthesis beyond the iron peak

The reaction rates for charged particle reactions decrease drastically with an increasing nuclear charge Z due to the Coulomb barrier. However, there is no coulomb barrier for neutrons and thus the neutron capture cross section is often quite large. This means that neutron captures provide a mechanism for nucleosynthesis beyond iron. The elemental abundances beyond iron can be attributed mainly to the slow and rapid neutron capture processes (s- and r-process, overall contribution to abundances: each $\sim$50%), with some contribution ($\sim$1% of overall abundances) from p-processes, mainly the γp-process, a photodisintegration process, which is responsible for the synthesis of several proton-rich isotopes.
When exposing seed nuclei to a neutron flux, the occurring reactions depend on the neutron capture cross-sections and beta decay half-lives of the involved nuclei. In the s-process, most beta decay rates along the path of nucleosynthesis are much higher than the average neutron capture rate: $\lambda_\beta << \lambda_n$. This means that the path of the s-process follows closely along the valley of stability. The s-process cannot synthesize isotopes heavier than ^{209}Bi, because heavier isotopes along the s-process path are unstable towards alpha decay.
In search for a nucleosynthesis process that has the ability to create the heaviest nuclei observed in nature, we must consider the r-process.

1.1.3 r-process

The classical r-process

The r-process was one of the eight nucleosynthesis processes originally proposed in 1957 by Burbridge, Burbridge, Fowler and Hoyle in their famous paper known as B^2FH [2] and Cameron [3]. It was suggested then, that seed nuclei (mostly iron) are exposed to a significant neutron flux on a short timescale, such that (n,γ) reaction rates are much higher than beta decay rates of the newly created nuclei. The path of nucleosynthesis then proceeds to very neutron-rich isotopes until photo disintegration (γ,n) rates can compete with the successive neutron captures. Assuming a (γ,n)$\leftrightarrow$ (n,γ) equilibrium within isobaric chains is referred to as the *waiting point approximation*. The abundance distribution within such an isobaric chain can be calculated using the nuclear Saha equation. Waiting points for the abundance flow are represented by isotopes with even N and significant abundance. At these waiting points, β^--decays transport matter from one isotopic chain to the next, however, slowly enough not to affect the flow equilibrium within isotopic chains. A special case occurs, when a magic neutron number is reached. The Q-value for a successive neutron capture on a N-magic nucleus is small, the corresponding reaction rate low. These nuclei also represent waiting points. Alternating β^--decays and neutron captures allow the r-process path to proceed upward in the nuclide chart.

The processes discussed above can be seen as the basic building blocks of the r-process path and are illustrated in figure 1.3. In the classical r-process, we assume that the temperature and the neutron flux are constant in time. Besides, the neutron exposure ceases instantly, and the neutron-rich isotopes undergo successive β^--decays (A=const.) until a stable isotope is reached. For each value of A, the r-process produces one stable (or long-lived) isotope if we do not take the effects of delayed neutron emission into account. If that isotope does not lie on the s-process path, and is thus only synthesized in the r-process, it is called a *r-only isotope*.

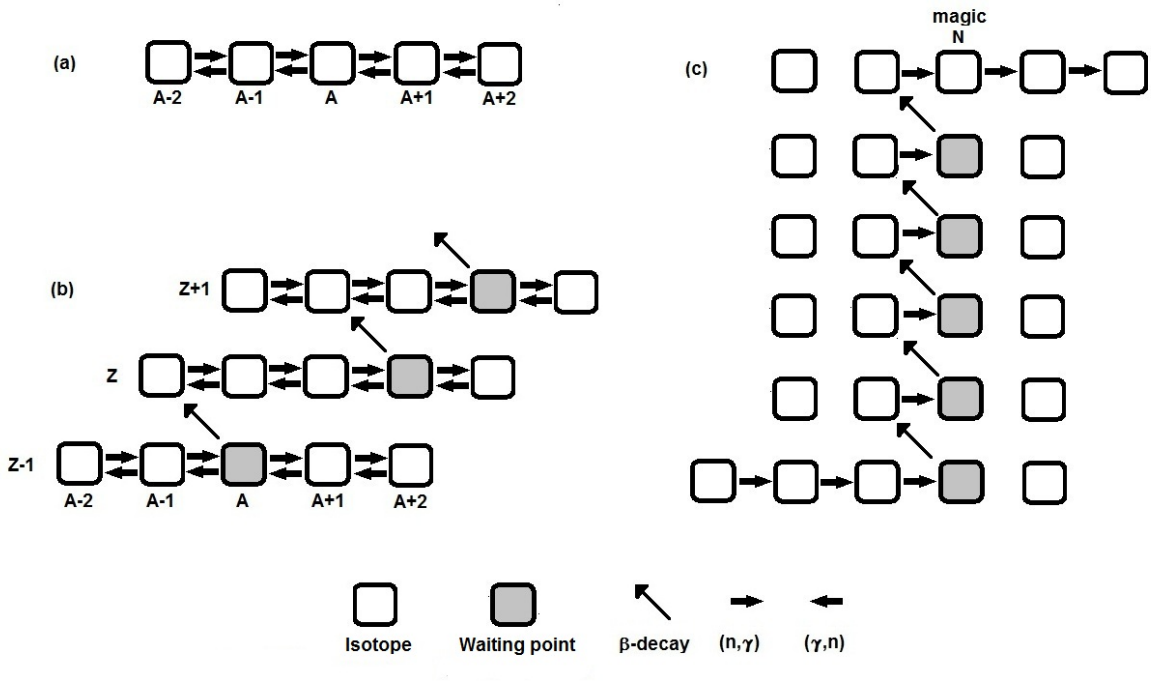

Figure 1.3: Basic building blocks of the classical r-process. (a) shows an isotopic chain in equilibrium. In (b), waiting point nuclei allow beta decays to transfer matter from one isotopic chain to the next. (c) depicts the influence of a closed neutron shell on the r-process path.

r-process calculations

For a specific r-process situation with given temperature T, free neutron number density N_n, and total neutron exposure $\tau = \int N_n(t)dt$, the final isotopic abundance distribution can be calculated only if the properties of the nuclei along the nucleosynthesis path are known.

The Q-values for (n,γ) reactions provide isotopic equilibrium abundances, while the total elemental abundance is determined by the total β^- decay rate λ_Z of an element. In the region of very neutron-rich isotopes involved in the r-process, only little experimental data are available. Even using radioactive beam facilities, the determination of masses and half-lives of very neutron-rich isotopes is difficult.

R-process simulations have been done for different mass models; an example can be seen in figure 1.4.

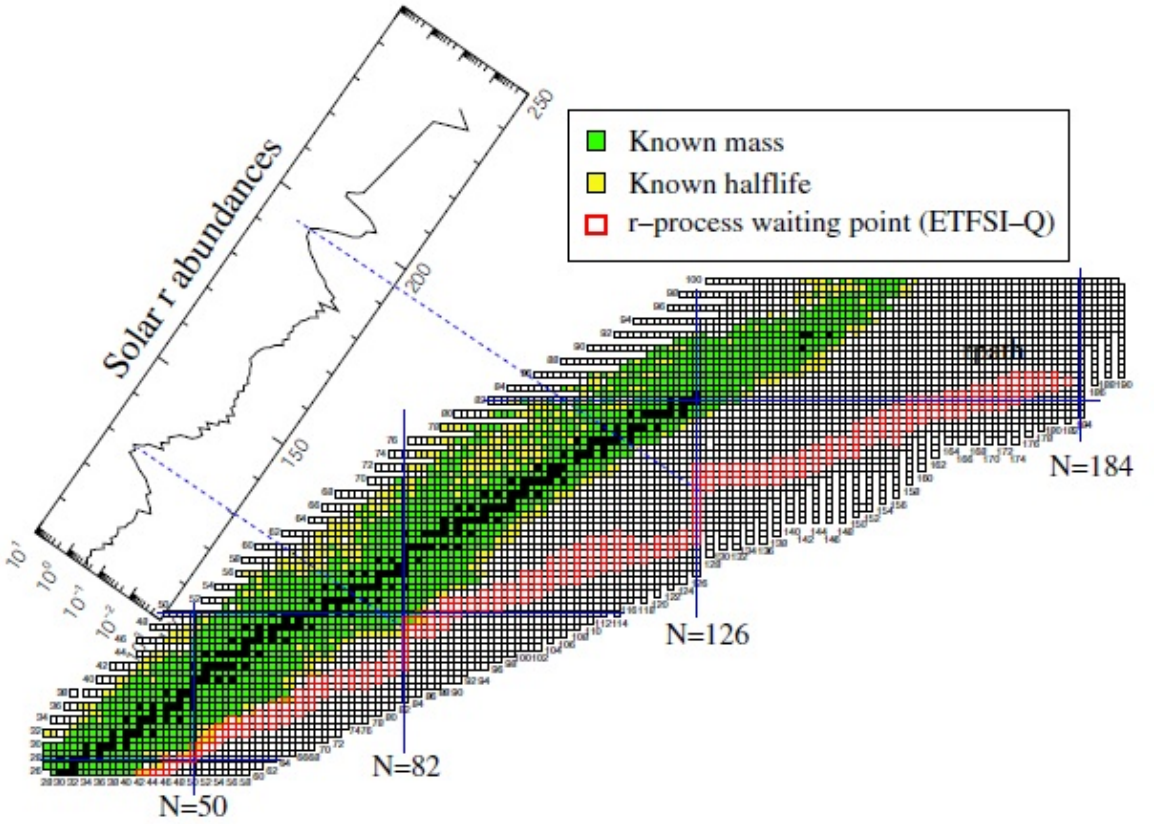

Figure 1.4: Illustration of the r-process path (red) and the effect of magic neutron numbers N=50,82,126 on the solar abundance. Taken from [4], based on ETFSI (Extended Thomas Fermi and Strutinsky Integral) mass model with special treatment of shell quenching [5].

For classical r-process calculations to get close to the solar abundance distribution, a superposition of neutron exposures is used. As a result, the r-process does not proceed along a narrow path, but rather along a broad boulevard [6].
The difficulty of predicting abundance distributions for the r-process in simulations increases with the number of uncertain quantities. It is thus impossible to create accurate r-process simulations for the mass region of superheavy elements. This also means that it cannot be excluded that superheavy elements are created in the r-process.

Astrophysical sites

The astrophysical site(s) for the r-process have not been identified with certainty. The requirement for such an astrophysical scenario is an extremely high neutron flux $N_n > 10^{20} cm^{-2}$ over a timescale of a few seconds at high temperature (few GK).
Among the oldest stars in our galaxy are metal-poor halo stars. Here, metal refers to any element heavier than lithium. Observations of these stars show that the abundance of r-only isotopes with A>135 in these stars is very similar to that in our sun. Since these metal poor stars cannot have synthesized these isotopes themselves, their progenitors must have produced them. This links the r-process to an early time in the evolution of our galaxy, and the corresponding r-process site seems to be related to massive stars. In the case of our sun, the observed r-process material in the photosphere dates back to the time before the solar system formed from the remains of a supernova explosion. This can be seen as another hint that massive stars and their explosions could be r-process sites.
There have been many different suggestions for astrophysical r-process sites, including the prompt hydrodynamical explosion of a type II supernova with a progenitor star of $8M_\odot \leq M \leq 10M_\odot$ [7, 8], the accretion disk flows in black hole - neutron star mergers [9], and explosions of low mass neutron stars [10].

An interesting candidate is the merging of two neutron stars [11, 12]. Although calculations show, that such an event can result in r-process nucleosynthesis, it is very rare. Thus, if it is the only r-process site, we would be able to observe a certain clumpiness of r-process material, which has not been confirmed. But at least a contribution of neutron star mergers to r-process nucleosynthesis has to be considered.

The most promising candidate is the neutrino-driven wind scenario in type II supernovae [13]. When a massive star approaches the end of its lifetime, the nuclear fuel in its center is used up and the star's core consists mostly of isotopes in the iron region. After this energy source ceases, the lack of pressure results in a contraction of the surrounding shells, and ultimately to a supernova explosion, which is accompanied by a neutrino-driven wind emanating from the proto neutron star that has formed in

the center of the star, providing r-process conditions.

In nature, it is likely that the observed r-process abundances contain contributions from more than one astrophysical site. In the future, further modeling and observations can provide better limitations on the choice of r-process sites and their respective contributions.

1.2 Theoretical approach

The heaviest known stable isotope is ^{208}Pb. The stability of this nucleus is due to the closed proton and neutron shells at Z=82 and N=126 respectively. Important questions arise: Where are the next closed proton and neutron shells? Are the shell effects strong enough to stabilize superheavy nuclei (SHN) against radioactive decay, creating an island of stability?

Theoretical predictions for the half-lives of SHN have proven to be challenging. One of the problems is the fact that the stability of a nucleus against spontaneous fission does not automatically provide it with a long half-life. The partial half-lives for alpha and beta decay also have to be considered.

For a theoretical description of the properties of superheavy nuclei (SHN), a purely macroscopic approach, based on the liquid drop model [14], is insufficient, because it does not take shell effects into account. Deformed and spherical shell closures provide increased stability against radioactive decay. The first semi-empiric approach was made by Myers and Swiatecki in 1966 [15]. They predicted an island of stability centered around Z=126 and N=184.

Improved semi-microscopic approaches, which take pairing and shell effects into account, for example a macroscopic-microscopic model, were developed. Over the next years, Z=114 and N=184 were established as spherical shell closures by several groups, e.g. Mosel and Greiner (1969) or Fiset and Nix (1972). However, the uncertainties in these calculations were very large, and the predicted half-lives of particular SHN were very far apart in different models. For example, the predictions for the half-life of ^{294}110 ranged from 10^4 to 10^9 years [16, 17].

Modern, purely microscopic models like relativistic mean field theory and the Hartree-Fock-Bogoliubov model predict a deformed neutron shell closure at N=162 and a spherical neutron shell closure at N=184. However different models still disagree on the location and strength of the next proton shell closure. While the original proposition Z=114 is still being considered, there have been other suggestions. In 1997, the calculations of Smolanczuk with a macroscopic-microscopic type model predict the most stable nucleus to be ^{292}Hs (Z=108) [18]. Gutpa et al. suggest an island of stability around N=184 and Z=126 with a second possibility Z=120 [19], while Bender et al. [20] suggest a broad region valley of shell stabilization around Z=120 and N=172-184 instead of an island of stability. The disagreements in the theoretical models call for experimental approaches.

1.3 Artificial creation

1.3.1 Fusion reactions

The first attempts to synthesize superheavy elements were made with neutron capture reactions [21]. Although the synthesis of elements up to Z=100 was possible in this way using captures of thermal and resonant neutrons and consecutive beta decays, the short spontaneous fission half-life of ^{258}Fm (T_{SF} = 0.3 ms) hindered the way to SHN. Another approach was necessary.

The production of SHN in the laboratory requires nuclear fusion reactions. Depending on the excitation energy of the compound nucleus, the fusion reactions are called *cold* (10-20 MeV) or *hot* (30-50 MeV). To reach the energies necessary for nuclear reactions, particle accelerator facilities are required. The identification of SHE created in fusion reactions can then be accomplished by measuring alpha-decay energies or by studying spontaneous fission events.

Cold fusion Since 1974, cold fusion reactions using ^{208}Pb and ^{209}Bi as targets have been used to synthesize heavy nuclei. Using heavy (m > 50u) projectiles reduces the excitation energy of the compound nucleus to 10-20 MeV, which dramatically increases its survival probability against spontaneous fission. It decays to the ground state via

emission of 1-2 neutrons and subsequent γ-emission. Fast techniques for separation and detection of newly formed nuclei are required. In 1975, a new setup featuring the UNILAC heavy-ion accelerator and the velocity separator SHIP at the Gesellschaft für Schwerionenforschung in Darmstadt provided the basis for the synthesis of elements 107-112 in cold fusion experiments [22, 23]. In general, SHN from cold fusion are relatively neutron-poor. It was also used to investigate the deformed shell closure N=162 [24]. Recently, the element 113 was synthesized at RIKEN in the cold fusion reaction [25]:

$$^{70}\mathrm{Zn} +^{209} \mathrm{Bi} \rightarrow^{278} 113 +^{1} \mathrm{n}$$

Note the relatively heavy projectile ^{70}Zn and the emission of only one neutron. Attempting to reach higher Z and at the same time approach the neutron shell closure N=184 is very difficult using cold fusion reactions, because it would require heavier projectiles. This is not only a challenge for accelerator technology, but also lowers the expected cross sections considerably (typically below 1pb for Z>113).

Hot fusion To increase the neutron-excess in the compound nucleus, more neutron-rich target materials, like ^{244}Pu, ^{248}Cm or ^{249}Cf can be used. The most advantageous projectile for hot fusion reactions is the doubly magic and neutron rich nucleus ^{48}Ca [26]. The SHE with Z=113-118 have been discovered with hot fusion reactions. As an example, we take a look at the reaction [27]:

$$^{48}\mathrm{Ca} +^{243} \mathrm{Am} \rightarrow^{288} 115 + 3 \cdot^{1} \mathrm{n} \rightarrow^{284} 113 + 3 \cdot^{1} \mathrm{n} +^{4} \alpha$$

The element 113 is produced as a decay product of element 115. However, we see that in comparison with the synthesis of the same element in cold fusion, a higher neutron excess is reached, providing a better chance to approach the predicted shell closures N=184 and Z=114.

1.3.2 Overview on discoveries

The synthesis of the elements $Z = 104 - 118$ was pursued mainly at four facilities:

- Joint Institute for Nuclear Research (JINR) in Dubna, Russia,
- Gesellschaft für Schwerionenforschung (GSI) in Darmstadt, Germany,
- RIKEN, Japan, and
- Lawrence Berkeley International Laboratory (LBNL), USA.

The first report of a successful synthesis of a transactinide element came from the JINR in 1964. They used a heavy ion cyclotron to accelerate ^{22}Ne ions onto a ^{242}Pu target. The experiment showed indications for the SHN ^{259}Rf (Z=104).
Since that time, isotopes of the elements 104 to 118 have been synthesized in hot and cold fusion experiments. Table 1.1 shows an overview of SHE in the range of $104 \leq Z \leq 126$. The discovery of several isotopes, like rutherfordium, was attributed to more than one laboratory. Especially during the cold war, the rivalry between the United States and Russia was reflected in the naming controversies for these elements, also known as the *Transfermium wars*. The IUPAC Commission on Nomenclature of Inorganic Chemistry decided on names for the elements 104 - 109 in 1997 [28].

To understand the connection between the nuclei synthesized in fusion reactions and a possible island of stability, it is necessary to look at the neutron-excess of these nuclei. The closed neutron shell N=184 puts the center of the island in a very neutron-rich region. However, the fusion of two stable isotopes cannot yield that kind of neutron excess. For example, the isotopes $^{263-277}$Hs (Z=104) have been synthesized in fusion reactions, but the hassium isotope with a closed spherical neutron shell, however, is be ^{292}Hs. Current fusion experiments thus do not have the capability to reach the island of stability.

Z	IUPAC name	Institute	Discovery	Reference
104	Rutherfordium	JINR + LBNL	1966-1969	[29, 30]
105	Dubnium	JINR + LBNL	1968-1970	[31, 32]
106	Seaborgium	LBNL	1974	[33]
107	Bohrium	GSI	1981	[34]
108	Hassium	GSI	1984	[35]
109	Meitnerium	GSI	1982	[36]
110	Darmstadtium	GSI	1994	[37]
111	Roentgenium	GSI	1994-2000	[38]
112	Copernicium	GSI	1996-2005	[38]
113	Ununtrium	JINR + RIKEN	2003-2004	[27, 25]
114	Ununquadium	JINR	1998-1999	[39]
115	Ununpentium	JINR + LBNL	2004	[27]
116	Ununhexium	JINR	2000-2001	[40]
117	Ununseptium	JINR	2010	[41]
118	Ununoctium	JINR + LBNL	2002-2006	[42]

Table 1.1: Overview on the SHE 104 - 118. The discovery of elements 113-118 in fusion reactions has been reported but not confirmed and thus still have placeholder names.

1.4 Search in nature

A number of techniques have been used to search for SHE in nature. The four most important examples are introduced in this section. To search for SHE in nature, experimental setups require both, an extremely high sensitivity and low background.

1.4.1 Neutron counting

SHN close to N=184 and Z∼110 are very neutron rich. This means that possible spontaneous fission events of these SHN are predicted to be accompanied by simultaneous emission of several neutrons [43]. The counting of single fission events with high neutron multiplicity is thus a sensitive technique that can be used to search for SHE in nature.

The relatively simple setups require no sample preparation, meaning that a wide variety of sample material can be examined easily. To reduce background, these experiments are carried out underground. The sensitivity can be increased by using large samples (up to several kg). This technique has been used since the early 1970s, and has been shown to achieve sensitivities in the order of 10^{-14} g/g using ^{3}He and liquid scintillation counters [44, 45].

A recent example of such a project is the SHIN (Search for Super Heavy elements In Nature) experiment. It is currently in progress at the LSM underground laboratory in Modane (France). They are using ^{3}He detectors to search for fission events of the SHE hassium (Z=108) in a pure osmium (predicted chemical homologue) sample. The experiment allowed them to set an upper limit of 10^{-14} g/g on the abundance of hassium in osmium, assuming a half-life of 10^9 years, with a 550g osmium sample in 2 years measurement time [46].

This example shows the main disadvantages of the neutron counting technique. Firstly, an assumption on the half-life of the SHN under consideration has to be made. A stable SHN could not be detected with neutron counting. The second disadvantage is the relatively long measuring time. In addition, the background for these experiments is not negligible. Random events with high multiplicity can occur over the long measurement times.

1.4.2 Fission tracks

Another approach to the search for SHE in nature is based on solid fission-track detectors. Local intense radiation caused by fission fragments can damage materials. In certain solids, like glass or plastics, these fission tracks can be made visible by etching with lead. Longer fission tracks correspond to more deposited kinetic energy and thus to a heavier mother nucleus. In minerals, fission tracks were allowed to accumulate over millions of years, which allows for a sensitive search for SHE with upper detection limits on the order of 10^{-16} g/g if the age of the sample is known [47, 48].

1.4.3 ICPMS

Recently, the group of A. Marinov reported the discovery of a superheavy element with Z=122 and A=292 in a sample of natural thorium with an abundance of (1-10)·10^{-12} in thorium [49]. They used inductively coupled plasma-sector field mass spectrometry (ICPMS) in this search. In this technique, the sample material is heated to several thousand degrees to create a plasma. Positively charged ions from the sample are then accelerated towards a mass spectrometer and identified. However, the results are disputed and could not be confirmed by Deringer et al. [50] using AMS. It is possible that the signals interpreted as SHE by Marinov et al. were molecular background, which is not entirely suppressed in ICPMS.

1.4.4 Accelerator Mass Spectrometry

The most important advantage of AMS over other techniques for the search for SHE in nature is the fact that AMS counts the number of atoms of a specific isotope directly. Thus one does not have to make assumptions on the half-lives of SHE to set upper abundance limits.

In 1977, in one of the first modern AMS experiments, Schwarzschild et al. [51] used the Brookhaven tandem accelerator to scan the mass range 345<A<355 for SHE in the sample material monazite. They reached a sensitivity of 10^{-10}g/g.

Another interesting AMS experiment was conducted using the tandem accelerator at the University of Pennsylvania in 1979 by Stephens at al. [52]. They searched for ^{294}Ds (Z=110) in its chemical homologue platinum and established an upper limit on the order of 10^{-11}g/g for the abundance of ^{294}Ds in platinum.

2 Accelerator Mass Spectrometry at the MLL

AMS is an ultrasensitive technique for isotope identification. An important difference between AMS and other Mass Spectrometry methods is the energy range, to which the particles are accelerated. For AMS, a particle accelerator (usually a Tandem Accelerator) is used to reach energies on the order of MeV (1MeV= $1.6 \cdot 10^{-13}$J) whereas in other MS systems, energies are typically on the order of keV. This high energy allows one to make use of nuclear detection methods for isobaric separation. Another important feature of AMS with a tandem accelerator is the complete suppression of molecular background that results from the electron stripping process occurring in the accelerator. This allows AMS to measure isotopic ratios for certain elements with a sensitivity of 1 part in 10^{15} to 10^{18}.
AMS was originally developed for measuring ^{14}C. The first AMS experiments using electrostatic accelerators (rather than cyclotrons) were carried out by two groups independently at the McMaster and Rochester Universities measuring ^{14}C in natural samples [53, 54]. Since then, many other long-lived radioisotopes have been detected using AMS, including ^{10}Be, ^{26}Al, ^{36}Cl, ^{41}Ca, ^{53}Mn, ^{60}Fe, and ^{63}Ni. AMS provides scientists of many different research areas with a unique tool for the determination of very low concentrations of long-lived radioactive and stable isotopes.

The experiments for this project were carried out at the AMS facility at the Maier-Leibnitz-Laboratory (MLL) of the Technische Universität München and the Ludwig-Maximilians-Universität München.
The setup consists of two beamlines: the GAMS (Gas-filled Analyzing Magnet System)

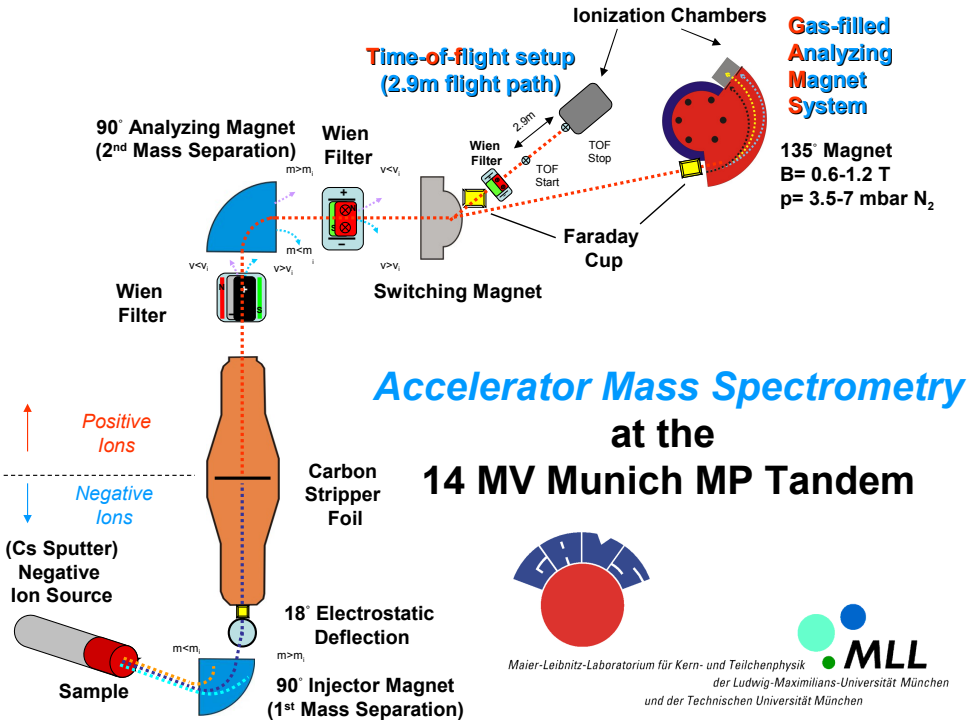

Figure 2.1: The current AMS setup at the Maier-Leibnitz-Laboratory in Garching with two beamlines.

and the TOF (Time Of Flight) spectrometer. For this experiment, the TOF setup was used. This section of the text serves to familiarize the reader with the components of the setup.

2.1 Samples

In all experiments for this project, we used threaded copper sample holders. Other sample holder materials were also available: graphite, silver, aluminum. However, copper was chosen, because it produces little background. Especially graphite proved problematic, because carbon tends to cluster formation over a wide mass range. Copper, on the other hand, with the two stable isotopes ^{63}Cu and ^{65}Cu cannot form pure copper-clusters in the mass range we scanned for SHE.

The sample material is hammered into a hole in the sample holder. We drilled holes

of 1.5 mm or 2 mm diameter and 2-3 mm depth into the holders. Smaller holes are better for mass resolution, but contain less sample material and are thus exhausted faster. For example, a sample holder with a 2 mm hole can contain approximately 100 mg of osmium powder, which is one of the sample materials we used. One sample can provide sufficient current for several hours before the sample material is exhausted. The prepared sample holder containing sample material is screwed onto a water-cooled rod and inserted into the ion source, see figure 2.2.

2.2 Ion source

The ion beam is produced by a Middleton type negative ion source with a spherical ionizer [55, 56].

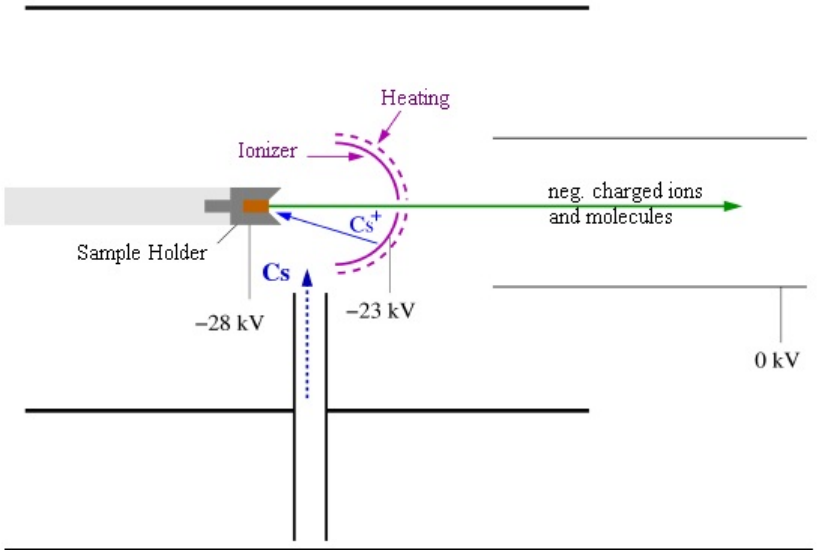

Figure 2.2: Schematic display of a high-current cesium sputter source of Middleton type [55, 56] with a spherical ionizer.

Cesium reaches the source from a heated reservoir. The Cs atoms are then ionized on a tantalum surface which is heated to roughly 1300 K. The positively charged Cs ions are then accelerated towards the sample by applying a 5 kV potential. The kinetic energy of the Cs ions is sufficient to eject particles from the surface of the sample. This

is referred to as sputtering. At this point, it is important to note that not only single atoms can be ejected from the sample in the sputtering process, but also molecules. These can either be sputtered as a whole or form after sputtering.
While sputtered neutral atoms and molecules may leave the ion source and are lost for the experiment, reducing the efficiency of the source, positively charged particles are trapped inside the sample holder due to the electrostatic potential. The required beam of negatively charged ions (molecular ions) is created as follows: Cesium sets down on the sample surface where the temperature is lower due to the water cooling. Sputtered atoms and molecules have to pass this layer of cesium where a charge transfer can occur because of cesium's low electronegativity. The negatively charged ions and molecular ions created in this way have the charge state -1; higher negative charge states are not formed. They are then accelerated out of the ion source with a 23 kV extraction voltage.

For the two beamtimes of the experiment, two slightly modified Middleton type ion sources were used.
In the first beamtime, we used a source with a tantalum housing, which serves as an ionizer. An underlying tantalum wire (diameter 1 mm) with aluminum-oxide insulation pearls is used for heating [57].
In the second beamtime, an older model was used. The ionizer in this source is made of coaxial tantalum wire coiled in a spherical shape which is also used for heating [58][56]. The main disadvantages of this design are the inhomogeneous ionizer surface and the high cost for the coaxial wire which has to be exchanged regularly.

2.3 Low-energy mass spectrometer

The ion beam then undergoes a preliminary mass separation. The negatively charged ions have the well defined energy of 28 keV and enter a 90 degree dipole magnet also referred to as the injector magnet. For an ion to pass through the magnet, the equivalence of the centrifugal force and the Lorentz force gives:

$$m \cdot v = e \cdot B \cdot r \tag{2.1}$$

Where m is the ion's mass, v its velocity, e the elementary charge, B the magnetic field, and r the radius of the ion's path. The current creating the magnetic induction can be regulated to allow ions of specific mass to pass. Note, that at this point, molecular background is still present. When, for example, the spectrometer is set to m=192 u, not only $^{192}Os^-$, but also molecular ions with the same mass can pass. After the mass spectrometer, the ions (and molecular ions) have a defined energy and mass (except for ions that suffered scattering processes). The ion beam is then deflected by a 18 degree electrostatic steerer, pre-accelerated with a 150 kV electrostatic potential, and then injected into the tandem accelerator with a total energy of
5 keV + 23 keV + 150 keV = 178 keV.

Mass resolution of the injection system: The current from the negative ion source can be measured using a Faraday cup that can be inserted into the beamline just before the ions would enter the tandem accelerator. By varying the magnetic field of the dipole magnet around the maximum current of a known isotope, the full width at half maximum (FWHM) of that peak can be determined. From equation 2.1 and E=$\frac{1}{2}$mv^2, we see that m $\propto$ B^2. This means that the mass resolution of the injection system can be defined as

$$\frac{\Delta m}{m} = 2 \cdot \frac{\Delta B}{B} \tag{2.2}$$

where m is the mass of the known isotope and B the magnetic field that yields maximum current at the Faraday cup and ΔB half of the FWHM. This means that two peaks of equal height can be resolved if they are at least half of the FWHM apart. Using a beam of $^{209}Bi^-$, the resolution has been determined to 1:316. This means that even for the high masses of SHE (around 300), the injection system is still able to resolve mass differences of 1 u.

2.4 Tandem accelerator

The facility includes a 14MV MP Tandem Van-de-Graff accelerator. The 25 m long tank contains 7 bar SF_6 serving as insulating gas. The negative ions enter the tandem accelerator and are accelerated towards the high-voltage terminal in the center, which is at positive potential (in this experiment: 8-10 MV). They then pass through a foil stripper. For this experiment, we chose a foil thickness of 4 $\mu g/cm^2$ and used single foils only. When ions pass through it, several electrons are removed. Bohr's atomic model gives the rudimentary prediction, that any electron with an orbital velocity smaller than the velocity of the ion will be stripped. In reality, however, a charge state distribution is created. It depends on the atomic numbers of the ion and the foil and on the ion's velocity. The foil is assumed to be thick enough to produce an equilibrium charge state distribution, but thin enough not to cause serious energy straggling for the ions. A very important feature of this stripping process is the suppression of any molecular background. When a molecular ion passes through the foil, the delicate equilibrium between the binding electrons and the electrostatic repulsion of the nuclei is disturbed by the removal of electrons. This causes the molecular structure to break apart.
The positive ions are then accelerated again towards ground potential at the high energy side of the tandem. The total kinetic energy of the ions after leaving the tandem accelerator is

$$E = \frac{m_{ion}}{m_{mol.ion}} \cdot 178keV + (\frac{m_{ion}}{m_{mol.ion}} + q) \cdot e \cdot U \tag{2.3}$$

for ions that reached the terminal as molecular ions, and

$$E = 178keV + (1 + q) \cdot e \cdot U \tag{2.4}$$

otherwise. Here, m_{ion} and $m_{mol.ion}$ are the masses of the ion and the injected molecular ion respectively, e the elementary charge, q the integer charge state produced in the stripping process, and U the applied terminal voltage. Typical charge states in this experiment range from 5+ to 11+, while typical energies are on the order of 100 MeV. Upon leaving the accelerator, the ions pass another 90 degree dipole magnet, the magnetic spectrometer. For our experiment, it was set to a magnetic field B = 1450 mT.

This results in a fixed magnetic rigidity p/q, with the ion momentum p and charge state q. This allows one to select one of the charge states produced in the stripping process for the experiment.

2.5 New Wien-filter

The beamline is equipped with three Wien-filters. In a Wien-filter, an electric field $\vec{E}$ and a perpendicular magnetic field $\vec{B}$ create a Lorentz-force on passing ions with mass m, velocity $\vec{v}$ and charge state q. The force equilibrium yields

$$q \cdot B \cdot v = q \cdot E \qquad \Rightarrow \qquad v = \frac{E}{B} \tag{2.5}$$

This allows us to select a desired ion velocity by adjusting the electric field E for a fixed magnetic field B.
A part of this project was the upgrade of the beamline with the third Wien-filter, kindly provided by the Hebrew University of Jerusalem, Israel.

2.5.1 Installation

To make room for the new filter, the existing beamline had to be dismantled and rebuilt. The filter was installed so that it deflects the beam vertically. This was done intentionally, because it is favorable to have magnetic deflections along the beamline alternating in horizontal and vertical directions, resulting in optimal background reduction. To remove ions with wrong velocities that receive a velocity component in the vertical direction in the filter, a slit pair with a variable opening distance was installed 3.1 meters behind the Wien-filter. The slits pair's opening can be narrowed (typically to 6 mm) for precise configuration of the filter's effect on the beam geometry. During the experiment, the filter's magnetic field was left constant. It was adjusted by varying the electric field only. In this way, the constancy of the magnetic rigidity on the high energy side of the beamline is guaranteed.

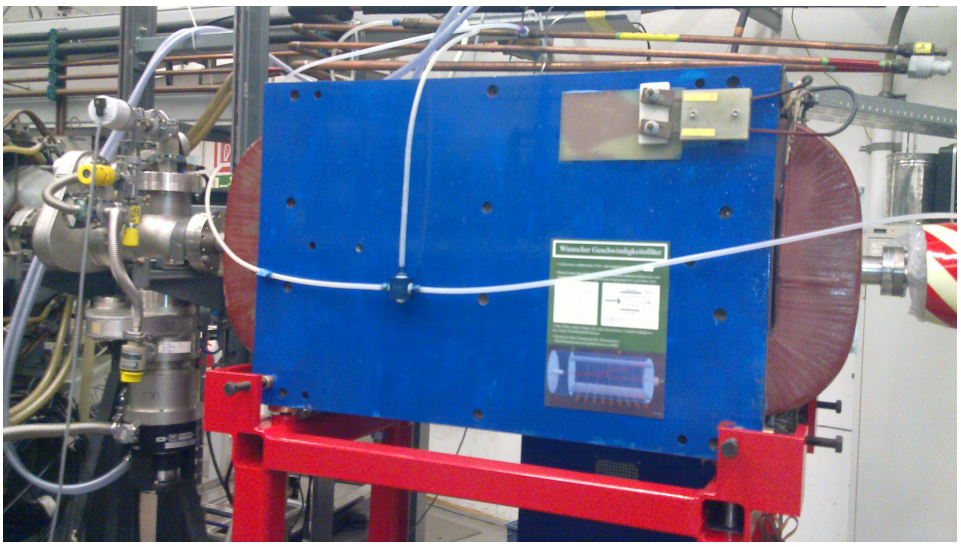

Figure 2.3: New Wien-Filter after installation in the I-20 beamline at the Maier-Leibnitz-Laboratory Garching.

2.5.2 Background reduction

To test the effect of the filter on the background, the beamline was set to A = 310 in the charge state 11+ and two runs were recorded with a raw platinum sample: one without and one with the new filter. Figure 2.4 shows the superimposed TOF spectra of the two runs. Most of the background arrived in the charge state 7+. The filter suppresses background events that arrive at the edges of the spectrum. The velocity window unaffected by the filter is approximately three masses wide (195-197 in the 7+ state). It would be ideal if the TOF value of $^{310}Ubh^{11+}$ was located in the center of this window. Unfortunately, it is located at a higher TOF. A possible explanation for this effect could be that the filter was slightly misaligned during this run, however, the TOF value of $^{310}Ubh^{11+}$ is still well inside the filters's window. It should be emphasized here that the counts arriving with roughly the same TOF as $^{310}Ubh^{11+}$ ions would are not signals from SHE, but from $^{197}Au^{7+}$ which has a similar TOF. In the case of the runs in figure 2.4, the new Wien-filter reduced the background for the experiment by a factor of two. However, depending on the exact kind of background for each specific setting of the beamline, this factor will vary.

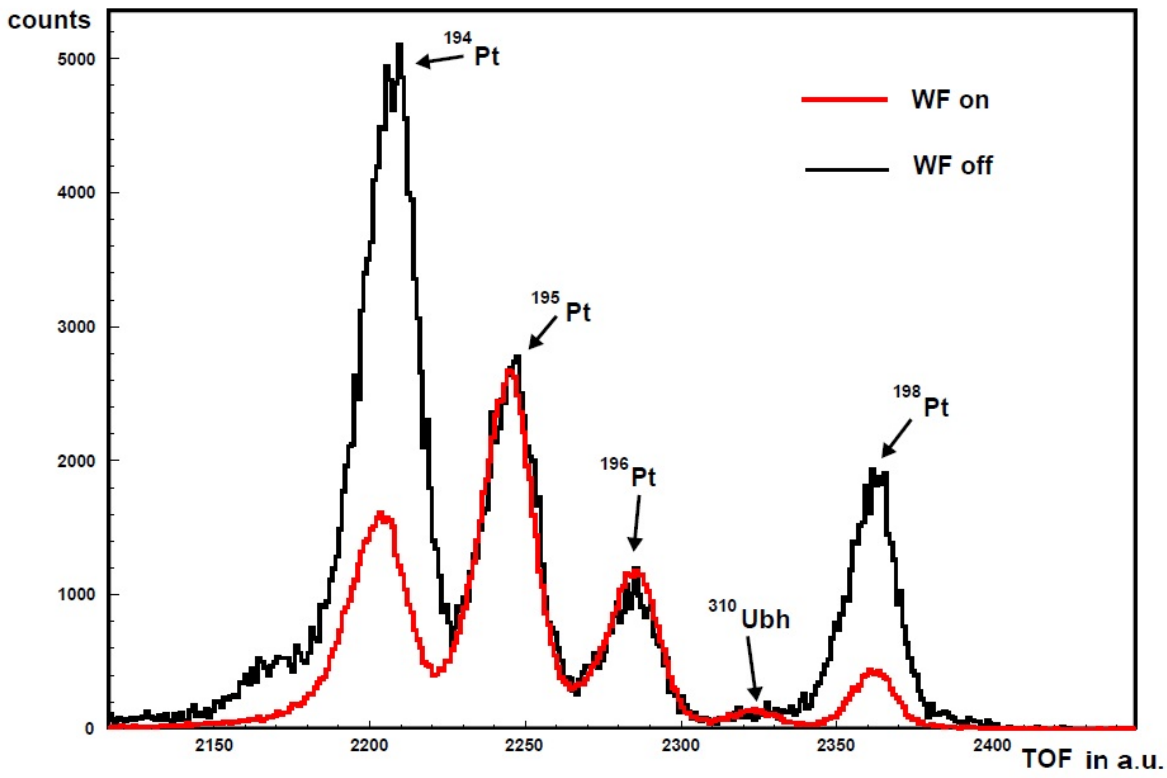

Figure 2.4: Superposition of two runs with $^{310}Ubh^{11+}$ settings. One with, one without the new Wien-filter. The spectra were scaled to take into account the different currents and measurement times during the runs. The filter suppresses events at the edges of the spectrum.

2.6 Detection system

The detection system of the experiment must be able to distinguish the desired isotope from others. To this end, the velocity (TOF signal), the energy loss in gas (E1,E2 and dE signals), and the remaining energy (Erest signal) of the isotopes are measured as described below and as can be seen in figure 2.5.

2.6.1 Ionization chamber

At the end of the beamline, the ions enter a gas-filled detector filled with 3-7 mbar isobutane gas through a thin mylar foil (0.9 μm) [59]. The gas pressure is regulated by a Piezo-valve and kept constant during the experiment. The anode is separated into

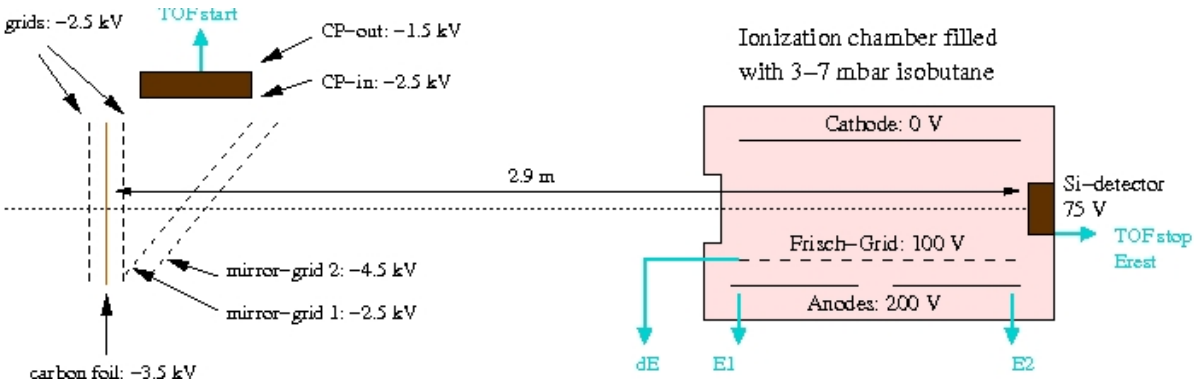

Figure 2.5: Detector setup including time of flight (TOF).

two parts, which allows one to measure the progress of energy loss and thus contains information on the ions' Bragg-curve. This provides another possibility for isotope identification. The ions collide with gas particles and ionize them. The ionization chamber is basically a capacitor, thus the electrons and positive ions created in this way drift towards the anodes and cathode respectively. Due to their lower mass, the electrons move faster than the positive ions ($\sim$ by a factor of 1000) and can be used to create a fast signal. Between anodes and cathode, another electrode, the Frischgrid (at +100 V) serves to make the signals from the electrons at the anode independent of the location at which they were created. The energy loss in the gas can then be measured with the signals E1 and E2 from two anodes at +200 V. The cathode (0 V) is coupled to the Frischgrid capacitively, thus the dE signal from the Frischgrid can be used to measure the total energy loss in the gas. The ions are then stopped in a silicon surface barrier detector with 400 mm^2 surface and a minimum depth of 60 μm with a bias voltage of +75 V. The kinetic energy of the ions is used up for the creation of electron-hole-pairs and creates the Erest signal.

2.6.2 Time of Flight

In the Time of Flight (TOF) measurement, the ions must produce both a start and a stop signal at fixed locations. This delivers a time information Δt, that can be translated into a velocity v with v= $\frac{L}{\Delta t}$, where L = 2.90 m is the TOF path.
The start signal is generated by a micro channelplate detector [60]. The ions pass through

a thin, flat Lensodel-type carbon foil (7.1 μm) [61] at a potential of -3.5 kV and eject several electrons from the foil. These electrons are then accelerated towards a grid at -2.5 kV in forward direction and then enter the field-free area between this grid and an electrostatic mirror grid placed at a 45 degree angle. A second electrostatic mirror grid at -4.5 kV bends the electrons out of the beam-axis and towards the channelplate detector where the electrons are multiplied and create a signal that is used as the TOF start signal. It must be considered that the ions loose energy passing through the carbon foil. This creates an energy and an angular straggling effect reducing the TOF resolution. In an attempt to find a compromise between TOF resolution (longer TOF path) and better energy resolution (shorter TOF path) a TOF path of $L = 2.9$ m was chosen. The angular straggling in the carbon foil was estimated using Ziegler's SRIM program [62]. This effect widens the beam-spot to $\sim$2cm at the entrance of the ionization chamber, which has an opening of 4 cm^2. Assuming a Gaussian distribution for the angular straggling, this means that not all of the ions in the beam reach the detector, this will be taken into account when the efficiency of the detection system is discussed in section 3.4. As TOF stop, we use the Erest signal from the silicon detector. Typical TOF times t_{TOF} are in the range of 300ns to 500ns.

2.7 Electronics and data acquisition

The signals from the detectors are amplified in pre- and main-amplifiers. The pre-amplified Erest signal is used to trigger the data acquisition for all other signals. This is done by a Constant Fraction Discriminator (CFD). The Erest signal is also run through a gate generator (GG) which supplies the gate to an analog-digital converter (ADC). All signals are run through main amplifiers and are then forwarded to the ADC. The TOF signal is generated with a time-amplitude converter which receives its start signal from the channelplate detector and the stop signal from the silicon detector, as previously mentioned. Figure 2.6 shows a sketch of the electronics.

It is necessary to distinguish real events from pile-up caused by two or more ions arriving almost simultaneously. A pile-up event generated by two ions of the same species can produce energy signals with up to twice the height of a single one. In the

case that two events are registered within 2-10 μs, a pile-up signal is generated and allows us to discard the event. Note, that events that are registered at the same time cannot be distinguished and thus cannot be discarded by pile-up rejection.

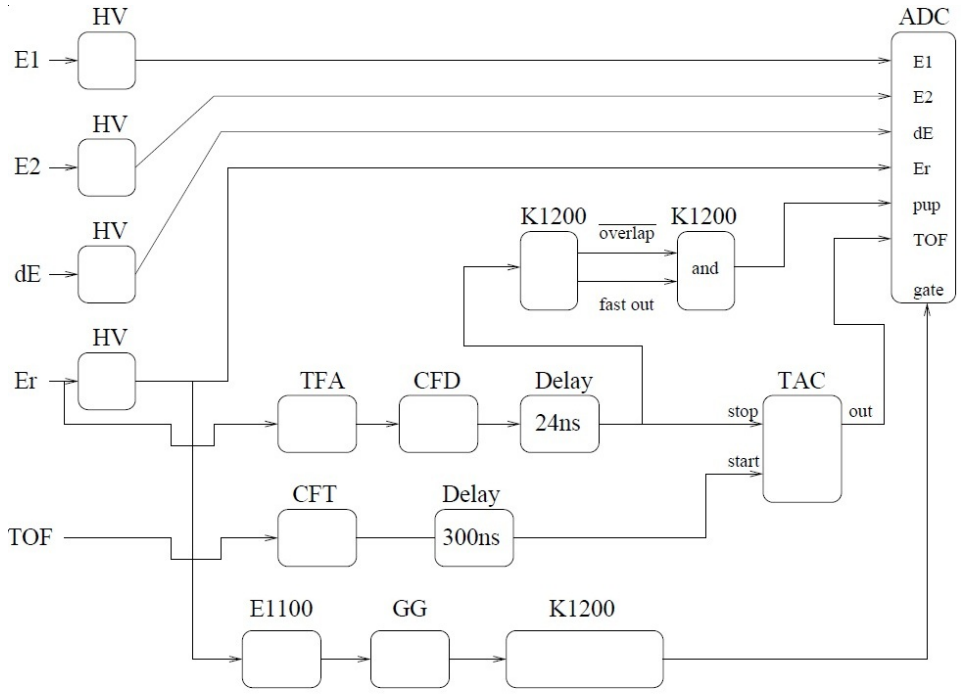

Figure 2.6: A sketch of the electronics used for signal processing in the experiment.

3 Preparation and implementation

3.1 Sample materials

The search for superheavy elements in nature is based on the possibility that one or more superheavy isotopes have a long enough half-life to exist in nature. Thus, it is reasonable to concentrate the search on isotopes which are predicted to be especially long-lived - doubly magic nuclei, as discussed in section 1.2. For this experiment, we assume a neutron shell closure at N=184. Since the predictions for the next closed proton shell after Z=82 range from $108 \leq Z \leq 126$, several superheavy candidates were chosen for the experiment.
The next step is choosing a sample material for AMS which has a chance of containing SHE. Chemically homologue elements can often occur together in nature, thus a suitable sample material for a specific SHE would be the chemical homologue.

3.1.1 Raw Platinum

We obtained a sample of raw platinum from the Impala Platinum Mines in South Africa [63]. The material is normally processed as depicted in the flow diagram in figure 3.1.

There are two main advantages in using raw platinum to search for SHE in nature. Firstly, a minimum of chemical processing increases the probability that SHE have not been filtered out. Secondly, since raw platinum contains different elements in the platinum group, it allows us to search for different SHE in one sample, because several superheavy elements are predicted to be chemical homologues to platinum group elements. The components of the raw platinum sample can be seen in figure 3.1.

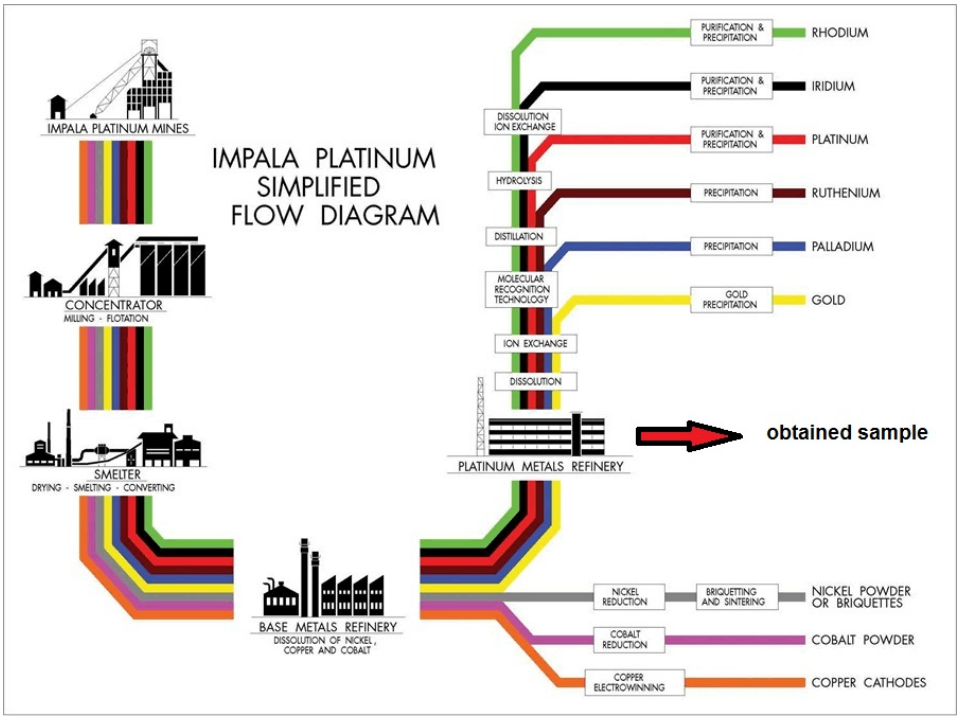

Figure 3.1: The flow diagram shows the chemical processing of the mined ore. Taken from [64].

Element	Pt	Pd	Au	Rh	Ru	Ir	Pb	As	Se	Te	Si	Ag	Os
Concentration [%]	32.3	19.9	1.2	5.8	6.4	2.2	1.9	1.4	0.1	0.7	1.8	2.5	0.1

Table 3.1: Contents of the raw platinum samples from Impala Platinum [63]. Note that the listed contents do not add up to 100%. Due to the lack of chemical processing of raw platinum, several other impurities are present but not listed here.

3.1.2 Single-compound samples

The main advantage of a pure sample is very simple - it contains more of the suspected chemical homologue. However, there is also a disadvantage. A pure material only allows the search for one specific SHE, because it only contains one possible chemical homologue. Also, chemical purification processes the materials have undergone contain the risk of filtering out SHE from the sample material. The sample materials osmium

and lead fluoride were chosen for the search for the SHE hassium and ununquadium respectively.

3.2 Tuning of the beamline

In order to allow a desired isotope to pass through the beamline and reach the detection system, the beamline has to be tuned. This is a routine process during the experiment and consists of the following steps:

- The injector magnet is tuned to the mass of the desired isotope.
- The tandem accelerator's terminal voltage is selected to provide the beam with the magnetic rigidity pre-determined by the high energy magnetic systems which remain unchanged to avoid hysteresis effects.
- The three Wien-filters are set to the velocity of the desired isotope. This is done by regulating the electric fields, while the magnetic fields remains constant.

3.3 Measurement principle

In order to check a sample for a small concentration of SHE, the chosen sample is placed in the ion source. At this point, one can choose whether to extract the desired isotopes as elemental ions or molecular ions. In some cases, molecular ions like oxides, carbides, and fluorides of specific elements yield higher currents. However, molecular ions undergo coulomb explosions at the stripping foil of the tandem accelerator leading to energy straggling. Thus, molecular ions are only injected when absolutely necessary as will be seen later in the case of lead fluoride in section 4.5.2.
A beam of the chosen reference isotope (e.g. $^{192}Os^{7+}$ extracted from $^{192}Os^{-}$ in an osmium sample) contained in the sample is focused along the beamline with several Faraday cups and the current is measured. The AMS system is then set to the mass and charge of a superheavy candidate as discussed in section 3.2. The data acquisition system records all occurring events with their corresponding signals (Erest,dE,E1,E2,TOF) during the run. The different signals can then be used to allocate events to specific isotopes. After

typically 1-2 hours, the run is ended and the beamline is tuned back to the reference isotope to measure the current at the Faraday cups again. The arithmetic mean $\bar{I}$ of the currents recorded before and after each run can then be calculated. This is necessary because current from the sample usually drops with time due to exhaustion of sample material.

3.4 Detection efficiency

The efficiency ϵ of the detection system is defined here as the probability for an ion that reaches the first Faraday cup in the dedicated beamline (after the switching magnet) to be observed in the detector. A beam of a stable isotope is produced and measured at the Faraday cup. For a charge state 10+, even with a low efficiency of 10%, typical currents of 10 nA correspond to a count-rate of 0.6 GHz in the detector. Unfortunately, foils and the semiconductor would be damaged by a beam of this intensity. Thus, the beam must be attenuated. For this purpose, three tungsten plates with 100μm holes that only transmit a fraction of the beam intensity can be put into the beamline: two plates with 1/1000 transmission and one with 1/33 [65].
The attenuated beam of a desired isotope X can then be let through to the detector, and the number of recorded events is used to calculate the efficiency ϵ with

$$\epsilon = \frac{A \cdot N_{ev} \cdot e \cdot q}{\bar{I} \cdot t} \tag{3.1}$$

where e is the elementary charge, N_{ev} the number of recorded events of isotope X, $\bar{I}$ the average current at the Faraday cup during a run (arithmetic mean), A the attenuation factor and t the measurement time.
During the beamtimes, the efficiency was determined several times for different isotopes. Typical values during the experiment ranged from $10\% \leq \epsilon \leq 40\%$.

Transmission from the low energy side to the detector Another interesting value is the probability, that an ion of a desired isotope that is injected into the tandem accelerator is registered in the detector. By comparing the currents measured by Faraday cups in front of the tandem and in front of the detection system, the transmission through

the tandem and the high energy side of the beamline can be calculated. Its value was ∼1 % throughout the experiment. This means that the total transmission from the low energy side of the tandem to the detector is $\sim 1\% \cdot \epsilon$. With an average efficiency $\epsilon = 25\%$, the average transmission during the experiment was $2.5 \cdot 10^{-3}$.

3.5 Setting upper abundance limits

If no events for a specific isotope Y are recorded, we can set an upper limit on its abundance in the sample. To this end, a reference current of a stable isotope X_{ref} is measured using a Faraday cup before and after each run. This allows us to estimate the average current $\bar{I}$ from the sample during the run. The total number N of X_{ref} atoms in the charge state q that could reach the Faraday cup during a run of duration t can be calculated to

$$N = \frac{\overline{I} \cdot t}{e \cdot q} \tag{3.2}$$

However, we have to take the efficiency of the detection system into account here. The total number of examined particles in the sample is

$$N_{eff} = N \cdot \epsilon \tag{3.3}$$

However, to link the current of isotope X to an abundance limit of isotope Y, we need to take into account, that different ions have different stripping yields in the tandem accelerator, as well as different behavior in forming negative ions (molecular ions) in the ion source.

The upper limit n_Y for the abundance of isotope Y in the sample material can be written as

$$n_Y = \frac{1.29}{N_{eff}} \cdot \frac{S_X}{S_Y} \cdot n_X \tag{3.4}$$

In this equation, n_X is the fraction of Isotope X in the sample material and the factors S_X and S_Y are the stripping yields, which means the probability for the formation of the selected charge state in the stripping process in the tandem accelerator for the isotopes

X and Y respectively. The factor 1.29 was included, because the detection of 0 events without any background corresponds to a maximum of 1.29 counts within a 1σ confidence level, as proposed by Feldmann and Cousins [66].
It should be noted that equation 3.4 does not take into account that the elements X and Y have a different ability to produce a negative current in the ion source, this will be explained in section 3.8.1.

3.6 Calibration of the detection system

When we look at a spectrum like figure 3.2, it is important to identify the isotopes that arrive in the detector and make a prediction of where to expect signals from SHE. This requires a precise calibration of the detection system.

3.6.1 Simulated signals

The time of flight signals are used to distinguish isotopes of different mass in the detector. To this end, it is useful to know the difference in signal height (or channel number) that corresponds to a certain time difference. For this purpose, a time calibrator was used to simulate start and stop signals with a difference of multiples of 10 ns.
The functionality of all other signals was tested using a pulser.

3.6.2 Calibration with known isotopes

Using attenuated beams of known isotopes, we were able to calibrate the detection system. We used $^{192}Os^{7+}$ from $^{192}Os^{-}$, $^{209}Bi^{9+}$ from $^{209}Bi^{-}$, $^{232}Th^{9+}$ from $^{232}ThO_2^{-}$ and $^{238}U^{8+}$ from $^{238}U^{-}$ beams from samples containing the respective elements. These data points then allowed us to extrapolate the expected energy and time of flight signals for SHE.

3.7 Background events

3.7.1 Isobars

In many AMS measurements, the sensitivity depends on the setup's ability to separate the desired AMS isotope from isobars, e.g. ^{60}Fe from ^{60}Ni. At the MLL, this can be achieved using the GAMS, see chapter 2. However, this is not a pressing issue for this experiment, because when searching for superheavy elements, any isobar detected would also be a superheavy element, and thus also be worth detecting.

3.7.2 Ions with similar m/q

The magnetic separation on the high energy side of the accelerator allows ions with a similar value of p/q to pass. Since the energy an ion receives in the tandem accelerator is roughly proportional to its charge, ions with similar m/q also obtain a similar velocity. These ions can pass through the filtering elements of the beamline on the high energy side and produce background. On the low energy side, however, most of these ions are filtered out by the injector magnet. Image 3.2 shows an example of a run with an osmium sample in a copper sample holder, where the AMS system was set to m = 292.2 u for the detection of ^{292}Hs in the charge state 11+, which means $m/q = 26.56$. This run was recorded with the original beamline, before its modification, which included the new Wien-filter. Only one Wien-filter was active at that time. This allows for a maximum of background to be visible. Although this is normally not desirable, it is practical for explanatory purposes. As in all following two-dimensional diagrams in this work, the energy signal from the silicon detector (Erest) is plotted against the TOF in arbitrary units.

The background events can be allocated to energy bands, which correspond to specific charge states. Isotopes with different mass arriving in the same charge state will have roughly the same energy, however, they can be distinguished by their velocity using the TOF signal.

- Osmium: The sample consists of osmium, so a lot of Os^- ions are produced in the ion source, some of which can pass through the injector magnet by forming

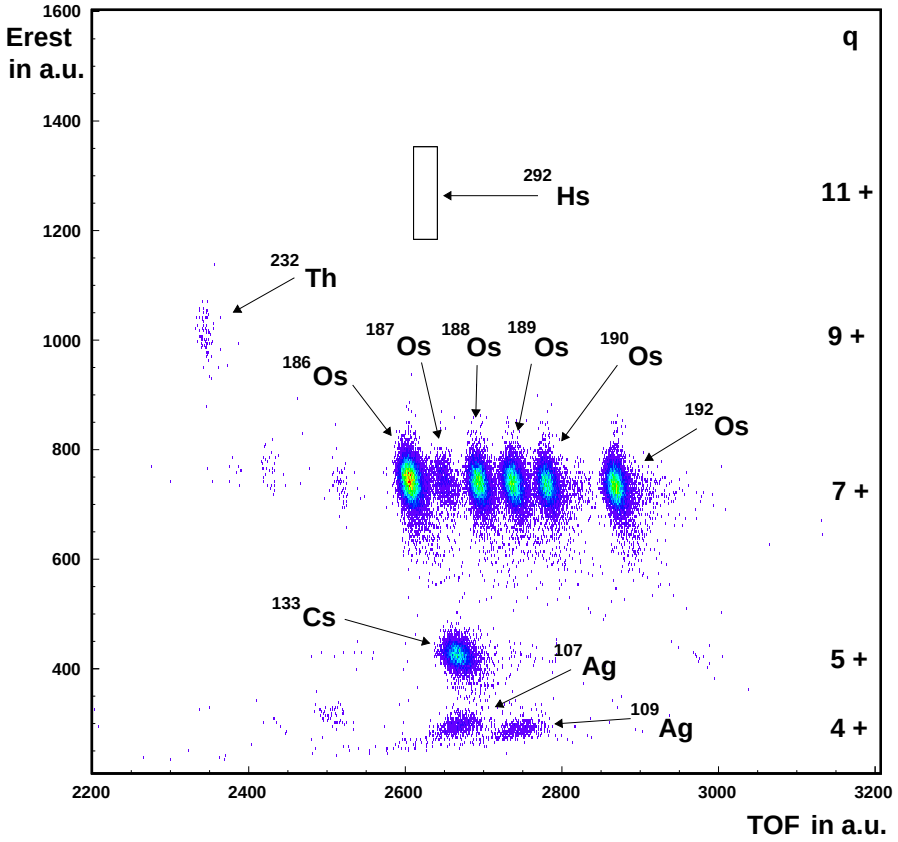

Figure 3.2: Run with an osmium sample and A=292, 11+ settings recorded with the original beamline, only one active Wien-filter. Higher intensity from purple to red. Erest and TOF signals in arbitrary units.

molecules with m∼292 u. In the charge state 7+, the Os isotopes $^{186-192}$Os have $26.57 \leq \frac{m}{q} \leq 27.43$, which allows them to pass through the high energy magnetic spectrometer. It is interesting to point out, that most background in this run was produced by ^{186}Os, although it has only an abundance of 1.59 % in Os. This can be explained by the fact that the m/q value of $^{186}Os^{7+}$ is closest to that of $^{292}Hs^{11+}$.

- Cesium: Some cesium background is visible in the charge state 5+ (m/q=26.60). It is difficult to avoid cesium from reaching the detector because cesium is used for the sputtering process in the ion source and is thus always present with the sample material. However, this background can be reduced by choosing a charge

state without a similar m/q and one should try to prevent the cesium ions from forming molecular ions with m∼292. To this end, carbon is avoided in the sample material and holders, to prevent the formation of Cs_2C_2 with m =290 u.

- Silver: The two stable silver isotopes ^{107}Ag (m/q=26.75) and ^{109}Ag (m/q=27.25) are also visible. They arrive in a charge state 4+. This can be explained by the fact that silver is one of the materials used for sample holders, and thus is always present in the ion source at trace level.

- Thorium: Several runs before, a thorium oxide sample was used to calibrate the detector. Thus, traces of thorium were still in the ion source. This explains that several events from ^{232}Th in the charge state 9+ were recorded.

For SHE, background events in the detector are ions with smaller masses and thus smaller charge state to match the p/q setting of the high energy spectrometer. The signal Erest is directly proportional to the energy deposited in the silicon detector. This means that background events can be clearly distinguished from real ones by their lower Erest signal.

3.7.3 Pile-up

As described before in section 2.7, pile-up events can create background. Figure 3.3 shows the effect of the pile-up rejection. Note that even with pile-up rejection, a few pile-up events with twice the energy of the other events remain because the two events creating the pile-up arrived simultaneously in the detector. For the pile-up rejection to function properly, the count-rate in the detector should not be too high (up to few hundred Hz). This makes it necessary to avoid settings that allow too much background to pass, this can be done by changing to another charge state if necessary.

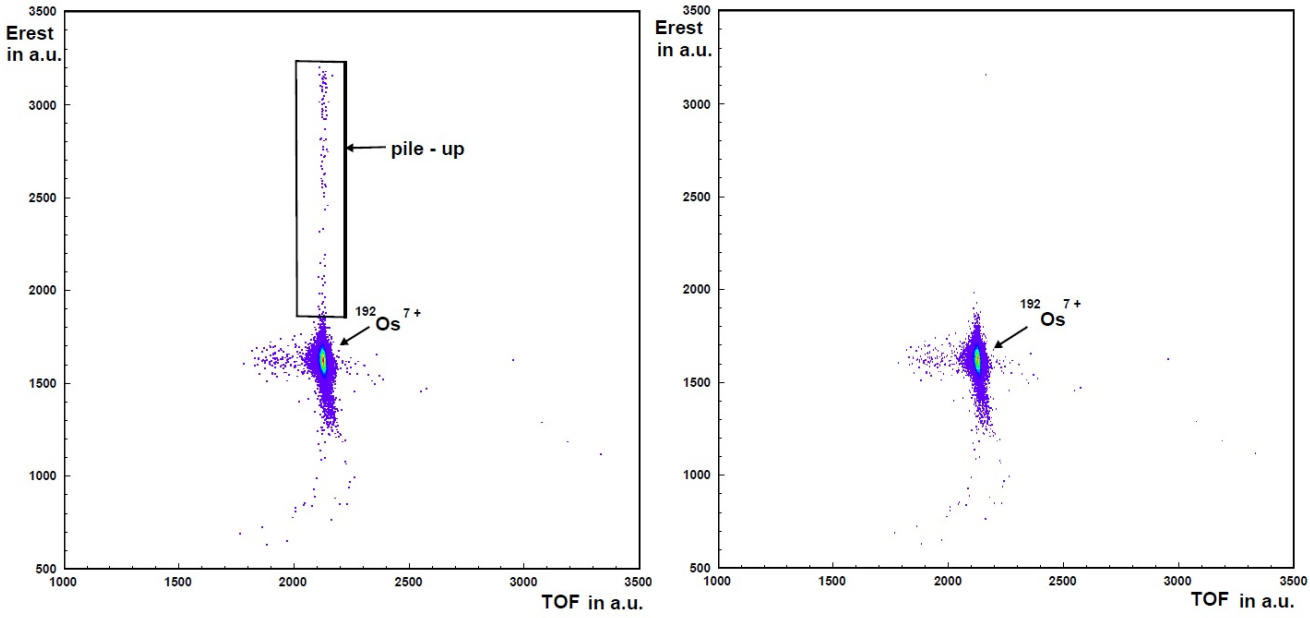

Figure 3.3: Pile-up rejection in a run with $^{192}Os^{7+}$ settings and an osmium sample (attenuated beam, factor $3.3{\cdot}10^{7}$). Erest and TOF signals in arbitrary units. Higher intensity from purple to red. Left side without - right side with pile-up rejection.

3.8 Considerations for AMS with SHE

3.8.1 Negative ion formation of SHE

As previously discussed in section 2.2, the key for the creation of a negative ion beam is the charge transfer of one electron from cesium atoms to atoms in the sample. The key quanitiy defining the efficiency of this process is the electron affinity of the desired ions. For this experiment, we make the assumptions that the electron affinity of hassium (eka-osmium) is similar to that of osmium (around 1 eV), and the electron affinities of the elements meitnerium, darmstadtium, roentgenium, and unbihexium are similar to that of platinum ($\sim$2 eV). These assumptions are however only valid, if the electron affinity of the SHE in the experiment are similar to those of their predicted chemical homologues.

3.8.2 Masses of SHE

The mass of an isotope must be known in order to tune the beamline as described in 3.2. To obtain precise masses of SHN, we must rely on models. For this experiment, the masses calculated by Smolanczuk [18] were taken. He predicts a mass excess of about 0.2 u for even-even nuclei with N=184 and Z=108-114. This mass excess was incorporated in the experiment by using the mass m[u] = A[u] + 0.2 for all SHN. So it should be noted, that whenever a mass reference like A=294 is mentioned in this work, it corresponds to a mass of m = 294.2 u.

3.8.3 Stripping yields of SHE

The high energy magnetic spectrometer selects one specific charge state. The yield of the charge states of SHE after the stripping process were calculated using the formulae provided by Sayer et al. [67]. Although these calculations are based on data for projectiles with Z<80 they can be extrapolated safely to heavier ions. To take the uncertainty due to this extrapolation into account, the calculated stripping yields were reduced by 20%. The resulting values for the yields were on the order of 15% throughout the experiment. The calculations predict the highest stripping yields for the SHE in the experiment at 10+ or 11+, depending on the element. However, it was not always favorable to blindly choose the charge state with the highest yield. One also has to consider which state produces less background as discussed in section 3.7.2.

3.8.4 Windows for SHE

In order to identify events from SHE, it is necessary to predict the expected signals they produce in the detection system. Since the tandem accelerator determines the energy, and thus the velocity, the expected signals can be calculated. The energy and velocity values are then converted into channel numbers by comparing them to reference isotopes, see section 3.6.2. The windows for SHE that can for example be seen in figure 3.2 are centered around these calculated values of the Erest and TOF signals. The width of the windows corresponds to a $\pm 2\sigma$ range, where σ is the typical width of the signals for known reference isotopes. It should be mentioned here, that while σ_{TOF} is constant,

σ_{Erest} is proportional to the height of the signal: $\sigma_{Erest} \propto Erest$. This has been included in the predictions.

4 Search for superheavy elements

We must consider that setting the AMS setup to, for example, A = 294 does not only allow the SHE Darmstadtium with Z = 110 and N = 184 to pass, but also others, like Hassium with Z=108 and N=186. But if we only consider the neutron number N = 184, we can allocate a specific element to each mass number with Z = A - 184.
In this section, the letter X refers to an arbitrary SHE and $\bar{I}$ denotes the average current of the reference isotope during all runs for each specific mass setting.

4.1 A = 292

4.1.1 Most likely candidate: Hassium

Hassium (or eka-osmium) is the chemical element with proton number Z=108. It was officially first synthesized at the Gesellschaft für Schwerionenforschung (GSI) in 1984 in Darmstadt (Hessen), ans was given the name hassium, derived from *Hessen* [35]. They managed to produce the isotope ^{265}Hs in the reaction ^{208}Pb+^{58}Fe$\rightarrow$^{265}Hs+^{1}n. Later in 1984, a group from Dubna was able to synthesize hassium isotopes as well and reported evidence for enhanced stability of Z=108 nuclei against spontaneous fission [68].
Until now, the hassium isotopes $^{263-277}$Hs have been observed, with half-lives ranging from milliseconds to seconds. As with all other fusion attempts to create superheavy elements, even the most neutron-rich isotope ^{277}Hs is still 15 neutrons away from the closed neutron shell N=184. In this experiment, we chose the potentially doubly magic isotope ^{292}Hs with Z=108 and N=184 for our search.
Hassium has been shown to be a chemical homologue to osmium [69, 70].

4.1.2 Search in Osmium

We used high purity Osmium powder purchased from Alfa Aesar [71]. Osmium has six stable and one primordial (^{186}Os - $T_{1/2} = 2 \cdot 10^{15}$ a) isotope. As a reference current, $^{192}Os^{7+}$ was chosen. ^{192}Os has a natural abundance of 40.78% in osmium.
During the first beamtime, only the first two Wien-filters were used because the installation of the third filter had not been completed yet. During the second experiment, all filters were active. No events that could be identified as A=292 ions were recorded. Figures 4.1 and 4.2 show examples of runs that were recorded with 10+ and 11+ settings respectively.

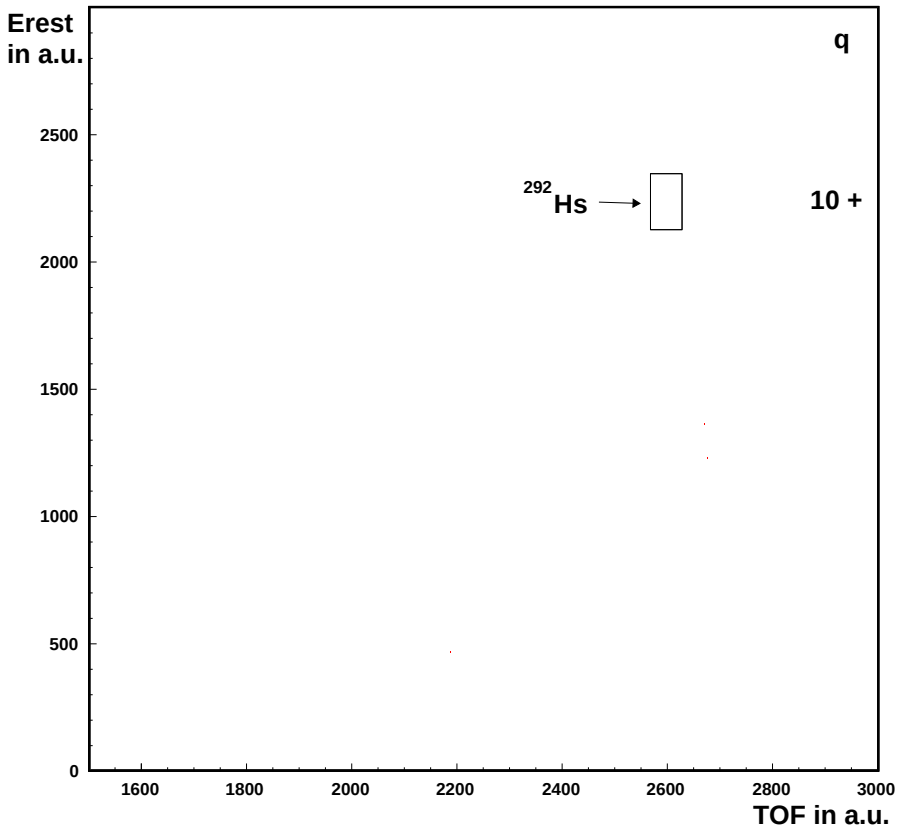

Figure 4.1: Example of a run with an osmium sample and A=292, 10+ settings. Only three background events were recorded.

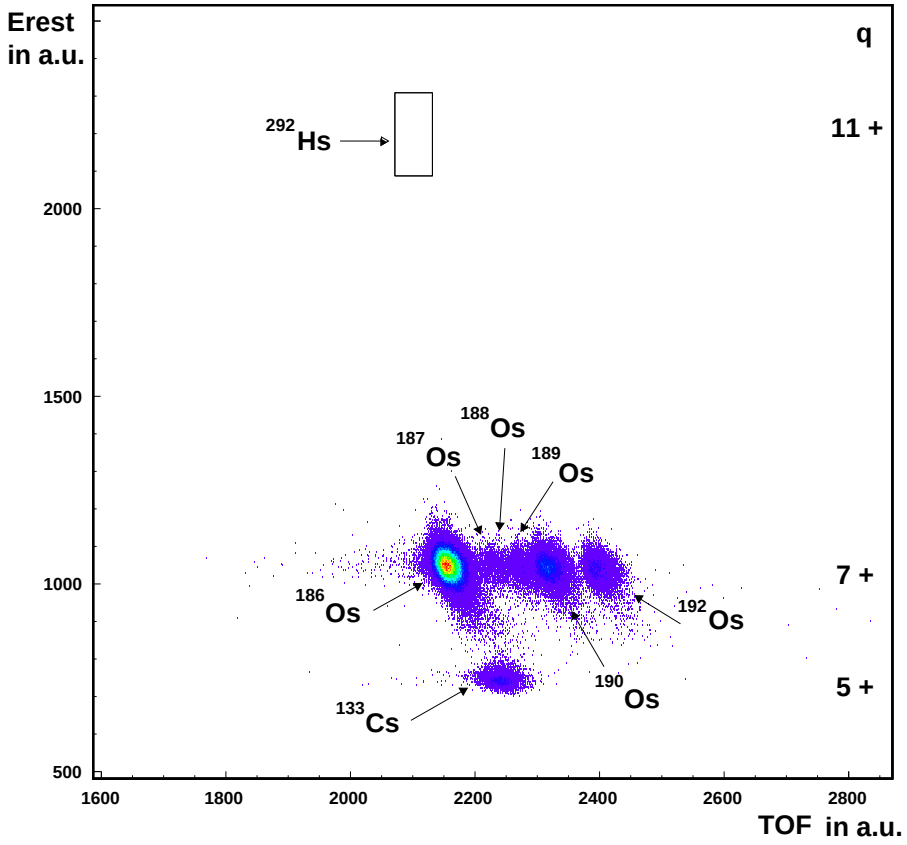

Figure 4.2: Example of a run with an osmium sample and A=292, 11+ settings. Higher intensity from purple to red.

Only three background events were recorded in the run with 10+ settings, while the 11+ run shows several interfering isotopes although the measurement time was on the same order for both runs. This difference results from the fact that for the 10+ settings for A=292, no other ions present in the beam can match the p/q value to be able to pass through the high energy side of the beamline. The advantage of the 10+ measurement is a cleaner spectrum with very little background, however there is also a disadvantage. Usually, the count-rate in the detector is proportional to the current of the reference isotope, thus a low but steady count-rate of background events is a way of monitoring the constancy of the current indirectly. This is not possible for the charge state 10+, because there is practically zero count-rate. Since both charge states, 10+ and 11+ have

their advantages, both were used in the experiment. An overview on the results can be seen in table 4.1.

Time [h]	$\bar{I}$ [nA]	ϵ	q(^{292}Hs)	b.g. [Hz]	events	u.l. ^{292}Hs/Os
25.6	10.74	0.20	11+	31	0	$3.8 \cdot 10^{-15}$
13.1	9.16	0.29	10+	0.01	0	$5.4 \cdot 10^{-15}$
Total					0	$2.2 \cdot 10^{-15}$

Table 4.1: Results for the search for SHE with A=292 in osmium. The table includes (from left to right) the measuring time, the average current of the reference isotope $^{192}Os^{7+}$, the efficiency, the charge state for the SHE, the background (b.g.) count-rate, the number of SHE events, and the resulting upper limit (u.l.) for the abundance of hassium in osmium on a 1-σ-confidence level.

4.1.3 Search in raw platinum

All other results presented here were obtained during the second beamtime using all three filters. Despite the low osmium concentration (∼0.1 %) in our raw platinum samples we also used it as a sample material for the search for SHE with A=292. This allowed us to look not only for ^{292}Hs, but also for other SHE with A=292. Unfortunately, the $^{192}Os^{7+}$ current was only 0.1 nA. This is why we decided to use the isotope $^{198}Pt^{7+}$ to obtain a reference current for all further measurements with raw platinum samples. Although is has only an abundance of 7.2 % in platinum, we chose it because its current can be identfied easily at the low energy side of the accelerator since the neighbouring Pt isotopes are unstable.

Figure 4.3 shows an example of a run with raw platinum. We can see some background from lead in the charge state 7+. Another source of background for this run can be seen in the charge state 4+. However, it covers a broad range in both TOF and Erest, which could mean that these are scattered ions, thus it is difficult to identify this background as a specific isotope. The most likely candidate would be ^{133}Cs.

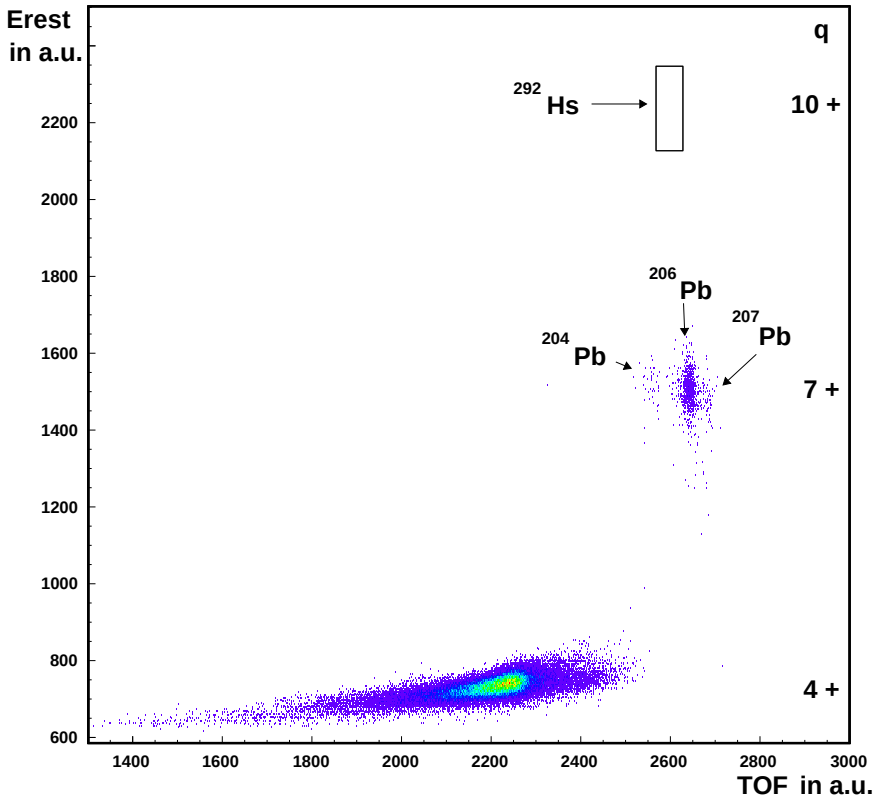

Figure 4.3: Example of a run with raw platinum and A=292, 10+ settings. Higher intensity from purple to red.

Time [h]	reference	$\bar{I}$ [nA]	ϵ	q(^{292}X)	b.g. [Hz]	events	u.l. ^{292}X/raw Pt
1.5	$^{192}Os^{7+}$	0.1	0.29	10+	10	0	$4.3 \cdot 10^{-15}$
2.3	$^{198}Pt^{7+}$	5.0	0.15	10+	9	0	$5.4 \cdot 10^{-15}$
Total						0	$2.4 \cdot 10^{-15}$

Table 4.2: Results for the search for SHE with A=292 in raw platinum. The table includes (from left to right) the measuring time, the isotope used as reference current, the average current of that isotope, the efficiency, the charge state for the SHE, the background (b.g.) count-rate, the number of SHE events, and the resulting upper limit (u.l.) for the abundance of SHE with A=292 in raw platinum on a 1-σ-confidence level.

4.2 A = 293

4.2.1 Most likely candidate: Meitnerium

The element meitnerium (also eka-iridium) (Z=109) was discovered in 1982 at the GSI in the reaction ^{209}Bi+^{58}Fe$\rightarrow$^{266}Mt+^{1}n and named in honor of Austrian physicist Lise Meitner. Several isotopes in the range of $^{266-278}$Mt have been observed since then. A possible chemical homologue to meitnerium is iridium.

4.2.2 Search in raw platinum

Again, ^{198}Pt^{7+} was used as reference current and the charge state 11+ was selected for SHN with A=293. Figure 4.4 shows an example of a run recorded with A = 293, 11+ settings. Most of the background was produced by Cs^{5+}, Ag^{4+}, and Os^{7+} ions. Additionally, a broad distribution of background over a wide TOF range can be seen. A possible explanation for this are scatterings on some part of the apertures along the beamline. More intense scatterings result in higher energy loss and thus longer TOF, explaining the drop of the distribution to the lower right of the spectrum. This effect might come from an unfortunate random interaction of the beamline elements causing the trajectory of a specific isotope to become unstable. However, this does not affect the sensitivity of our search for SHE, because all these background events can be clearly discarded by their low energy (Erest signal).
The results can be seen in table 4.3. The iridium content of 2.2 % in raw platinum also allows us to set an upper limit on the abundance of ^{293}Mt in iridium.

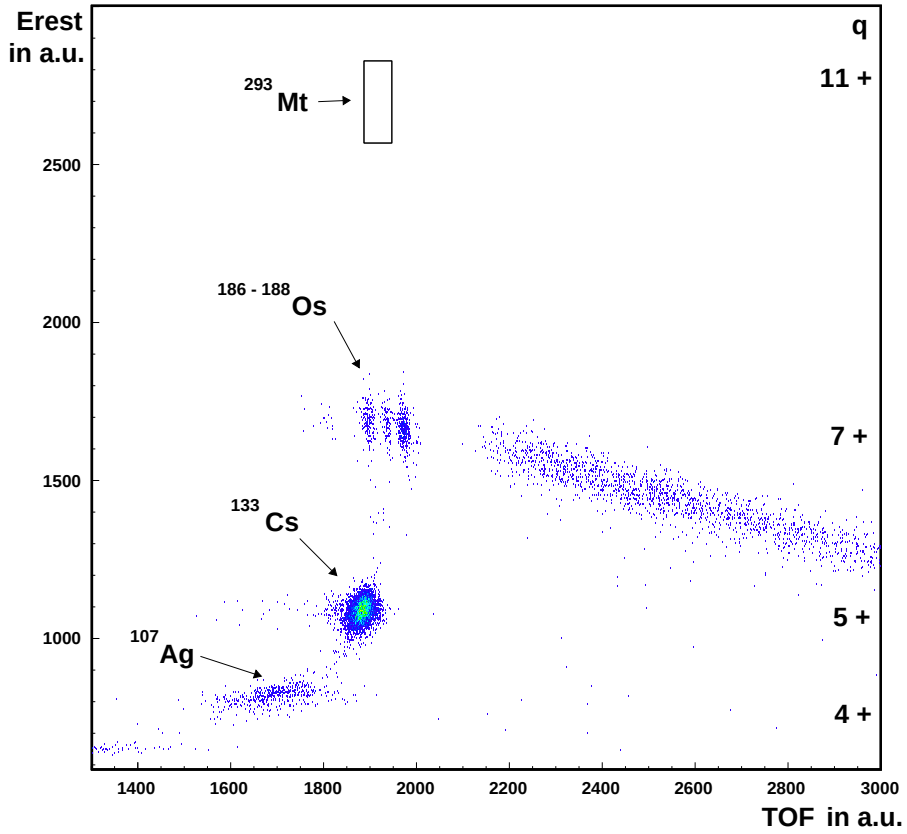

Figure 4.4: Example of a run with a raw platinum sample and A=293, 11+ settings. Higher intensity from purple to red.

Time [h]	$\bar{I}$ [nA]	ϵ	q(^{293}X)	b.g. [Hz]	events	u.l. ^{293}X/raw Pt	u.l. ^{293}Mt/Ir
4.2	6.7	0.27	11+	2	0	$1.2 \cdot 10^{-15}$	$5.5 \cdot 10^{-14}$

Table 4.3: Results for the search for SHE with A=293 in raw platinum. The table includes (from left to right) the measuring time, the average current of the reference isotope $^{198}Pt^{7+}$, the efficiency, the charge state for the SHE, the background (b.g.) count-rate, the number of SHE events, and the resulting upper limits (u.l.) for the abundance of SHE with A=293 in raw platinum and for Mt in Ir on a 1-σ-confidence level.

4.3 A = 294

4.3.1 Most likely candidate: Darmstadtium

Darmstadtium is the element with the atomic number Z=110. It was also discovered at the GSI, in 1994 [37] and named after the city of Darmstadt. Several isotopes in the range of $^{267-281}$Ds have been synthesized in hot and cold fusion reactions. Their half-lives range from milliseconds to minutes. A likely chemical homologue of darmstadtium is platinum, which makes it a good candidate for a search in raw platinum.

4.3.2 Search in raw platinum

Figure 4.5 shows an example of a run with A=294, 11+ settings. The background for these settings was quite similar to that of A=293, 11+ settings, so an explanation will be skipped here. The reader is referred to section 4.2. The high platinum content of 32.3 % in raw platinum also allows us to set an abundance limit of ^{294}Ds in Pt.

Time [h]	$\bar{I}$ [nA]	ϵ	q(^{294}X)	b.g. [Hz]	events	u.l. ^{294}X/raw Pt	u.l. ^{294}Ds/Pt
6.7	8.0	0.24	11+	17	0	$8.8 \cdot 10^{-16}$	$2.7 \cdot 10^{-15}$

Table 4.4: Results for the search for SHE with A=294 in raw platinum. The table includes (from left to right) the measuring time, the average current of the reference isotope ^{198}Pt^{7+}, the efficiency, the charge state for the SHE, the background (b.g.) count-rate, the number of SHE events, and the resulting upper limits (u.l.) for the abundance of SHE with A=294 in raw platinum and for Ds in Pt on a 1-σ-confidence level.

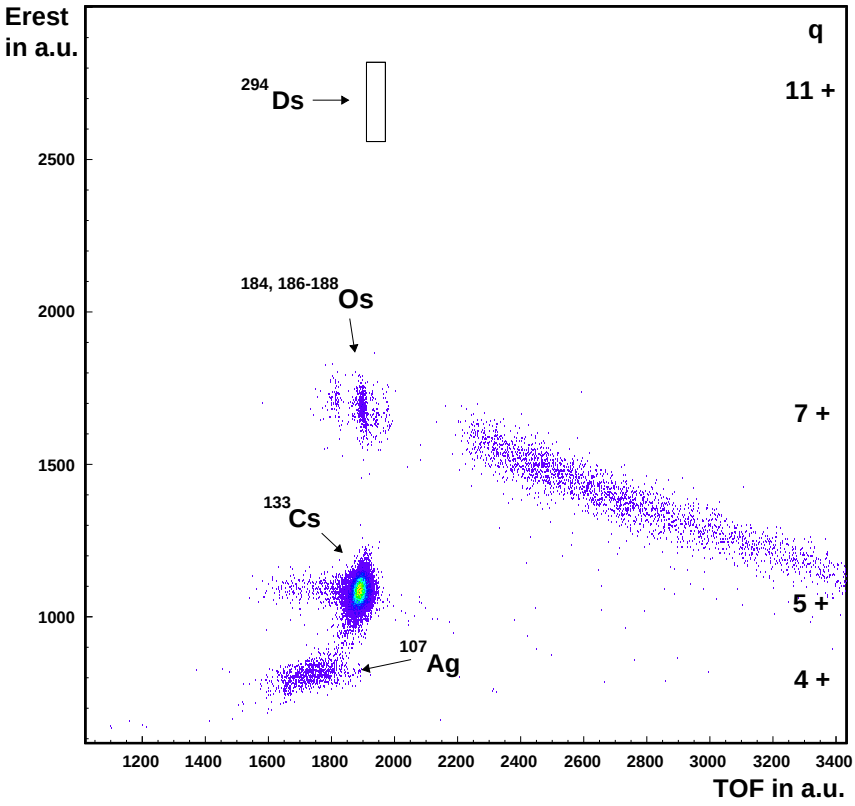

Figure 4.5: Example of a run with a raw platinum sample and A=294, 11+ settings. Higher intensity from purple to red.

4.4 A = 295

4.4.1 Most likely candidate: Roentgenium

Discovered in 1994 at the GSI in the cold fusion reaction ^{209}Bi+^{64}Ni$\rightarrow^{272}$Rg+^{1}n, Roentgenium (Z=111) has been suggested as a chemical homologue of gold [72], however, this remains to be confirmed. Again, to provide a variety of possible chemical homologues we used raw platinum samples. In addition to an abundance limit on SHE with A=295 in raw platinum, an upper limit for the abundance of ^{295}Rg in gold is provided.

4.4.2 Search in raw platinum

The charge state 10+ was chosen for the search for SHE with A=295. An example of a run with these settings can be seen in figure 4.6. Almost all of the background for this experiment arrived in the 7+ charge state. The lead content of our raw platinum samples was 1.9%. Due to the similar m/q value of lead in the charge state 7+ and A=295 in the state 10+, the lead isotopes ^{206}Pb, ^{207}Pb, and ^{208}Pb are responsible for most of the background.

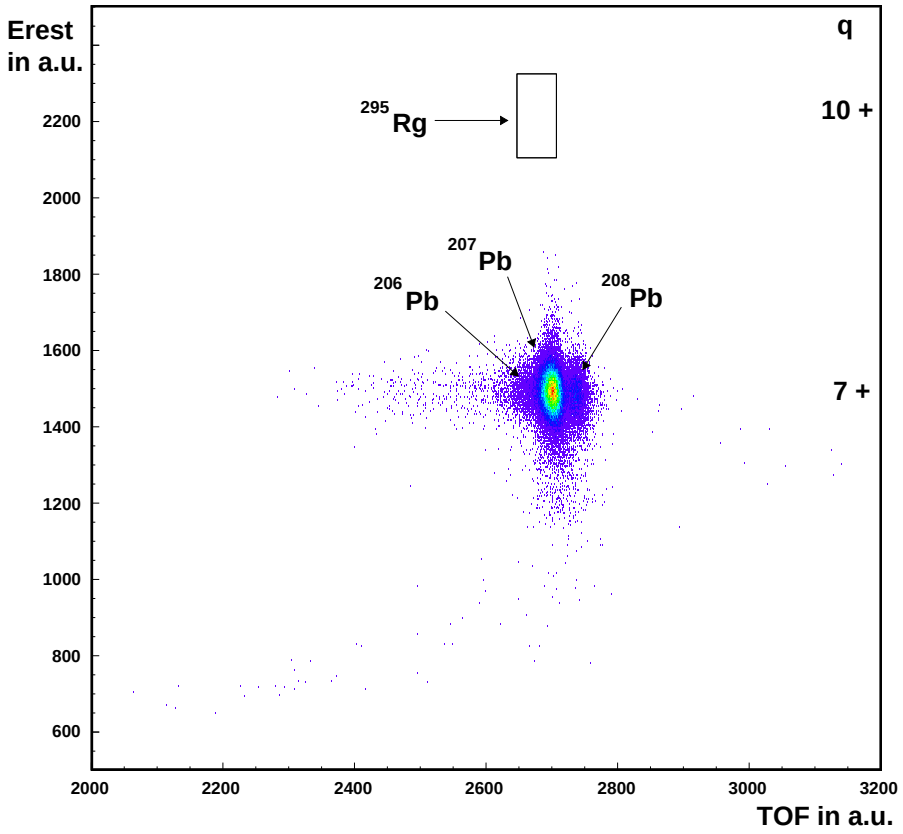

Figure 4.6: Example of a run with a raw platinum sample and A=295, 10+ settings. Higher intensity from purple to red.

Time [h]	$\bar{I}$ [nA]	ϵ	q(^{295}X)	b.g. [Hz]	events	u.l. ^{295}X/raw Pt	u.l. ^{295}Rg/Au
7.4	6.8	0.31	10+	6	0	$5.9 \cdot 10^{-16}$	$4.9 \cdot 10^{-14}$

Table 4.5: Results for the search for SHE with A=295 in raw platinum. The table includes (from left to right) the measuring time, the average current of the reference isotope $^{198}Pt^{7+}$, the efficiency, the charge state for the SHE, the background (b.g.) count-rate, the number of SHE events, and the resulting upper limits (u.l.) for the abundance of SHE with A=295 in raw platinum and for Rg in Au on a 1-σ-confidence level.

4.5 A = 298

4.5.1 Most likely candidate: Ununquadium

Since ununquadium is the chemical element with the often suggested proton shell closure Z=114, it is a very interesting candidate for the search in nature. It was originally proposed to have a chemical behavior similar to lead. This is why we decided to search for the element in lead. Recent data suggests that the chemistry of ununquadium is more noble-gas like, similar to radon [73]. However, at this point, it cannot be excluded that lead is a chemical homologue to ununquadium.

4.5.2 Search in lead fluoride

Lead does not produce a high enough current as a metallic ion. This is why we used lead fluoride as sample material. This was the only part of the experiment where the injection of molecular ion was necessary. PbF_3 produces the highest current [58].
We selected $^{208}Pb^{7+}$ as reference current. We assume that ununquadium forms a trifluoride with a mass of 355.2 u. The limited magnetic field of the injector magnet (1.14 T) forced us to reduce the sputter voltage from 5 kV to 4.25 kV and the extraction voltage from 23 kV to 20 kV. We assume a similar chemical behavior of ununquadium and lead. Thus, it is reasonable to attempt to extract $UuqF_3^-$ from the ion source.
Two 1 hour runs with pure lead fluoride were recorded. The current decreased by a

factor of 2 during each run. To prevent this quick exhaustion of the sample material, another two runs with lead fluoride mixed with silver powder (1:1 vol.) were recorded. Unfortunately, the current kept decreasing dramatically during the runs (25 nA down to 0.4 nA and 15 nA down to 0.5 nA). This behaviour was most likely due to an excess of fluorine in the ion source. For these runs, the average current was calculated using an exponential fit $I(t) = I(t = 0) \cdot exp(-\lambda t)$ rather than the arithmetic mean. The resulting lower average current $\bar{I}$ in these runs has been considered in the results shown in table 4.6. An example of a run with a sample of lead fluoride mixed with silver and A=298, 11+ settings can be seen in figure 4.7. The majority of the background for this run was $^{109}Ag^{4+}$.

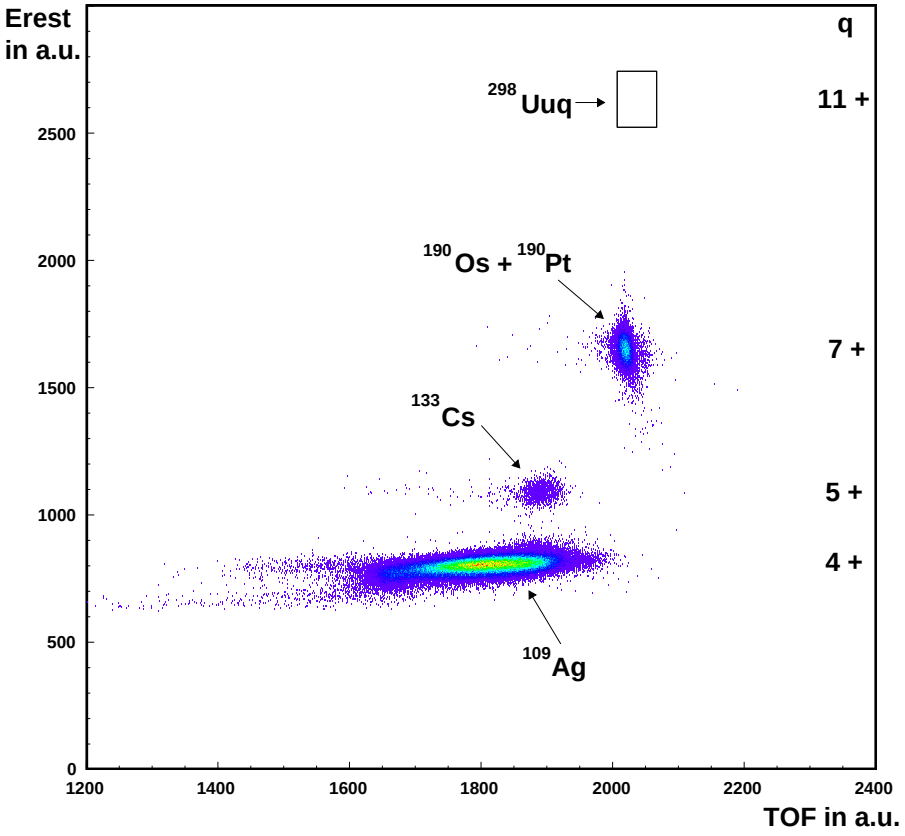

Figure 4.7: Example of a run with a lead fluoride sample and A=298, 11+ settings. Higher intensity from purple to red.

Time [h]	$\bar{I}$ [nA]	ϵ	q(^{298}Uuq)	b.g. [Hz]	events	u.l. ^{298}Uuq/Pb
5.2	15.1	0.26	11+	11 (43)	0	$1.5 \cdot 10^{-14}$

Table 4.6: Results for the search for SHE with A=298 in lead fluoride. The table includes (from left to right) the measuring time, the average current of the reference isotope $^{208}Pb^{7+}$, the efficiency, the charge state for the SHE, the background (b.g.) count-rate for pure PbF_2 samples and in brackets for PbF_2 mixed with silver, the number of SHE events, and the resulting upper limit (u.l.) for the abundance of SHE with A=298 in lead on a 1-σ-confidence level.

4.6 A = 310

4.6.1 Most likely candidate: Unbihexium

Unbihexium is a hypothetical chemical element with the proton number Z=126. The possibility of a proton shell closure cannot be excluded for this element, which makes it very interesting for the search in nature. Unfortunately, the chemical behaviour of unbihexium is mostly unknown [74]. This makes raw platinum a good sample candidate because it provides several possible chemical homologues unbihexium might be present with.

4.6.2 Search in raw platinum

We searched for SHE with A=310 in the charge state 11+. Figure 4.8 shows an example of a run with A=310, 11+ settings. Almost all of the background events arrived in the charge state 7+, mostly $^{195}Pt^{7+}$.

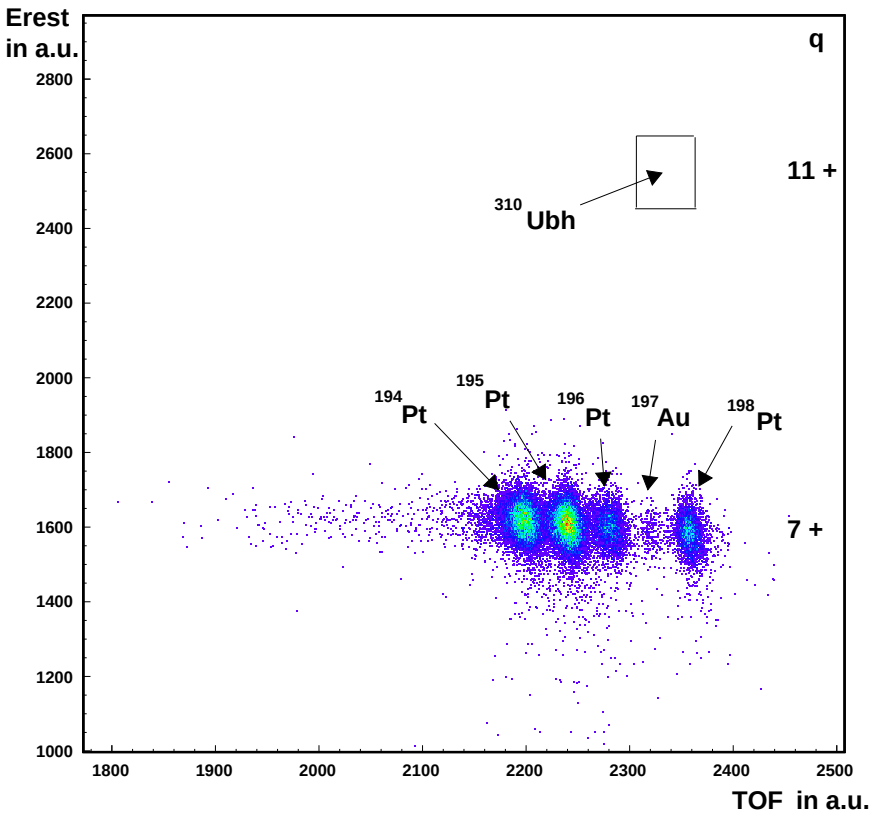

Figure 4.8: Example of a run with a raw platinum sample and A=310, 11+ settings. Higher intensity from purple to red.

Time [h]	$\bar{I}$ [nA]	ϵ	q(^{310}X)	b.g. [Hz]	events	u.l. ^{310}X/raw Pt
6.2	4.9	0.31	11+	33	0	$1.0 \cdot 10^{-15}$

Table 4.7: Results for the search for SHE with A=310 in raw platinum. The table includes (from left to right) the measuring time, the average current of the reference isotope $^{198}Pt^{7+}$, the efficiency, the charge state for the SHE, the background (b.g.) count-rate, the number of SHE events, and the resulting upper limit (u.l.) for the abundance of SHE with A=310 in raw platinum on a 1-σ-confidence level.

4.7 Discussion of results

4.7.1 Overview

In conclusion, an overview of the obtained results of the search for SHE is provided. The masses A=292-295, 298, and 310 were scanned. No events from SHE were detected. The resulting upper limits for the abundances of the SHE in the sample materials are summarized in table 4.8.

ratio	sample material	events	upper limit
^{292}Hs/Os	osmium	0	$2.2 \cdot 10^{-15}$
^{292}X/raw Pt	raw platinum	0	$2.4 \cdot 10^{-15}$
^{293}Mt/Ir	raw platinum	0	$5.5 \cdot 10^{-14}$
^{293}X/raw Pt	raw platinum	0	$1.2 \cdot 10^{-15}$
^{294}Ds/Pt	raw platinum	0	$2.7 \cdot 10^{-15}$
^{294}X/raw Pt	raw platinum	0	$8.8 \cdot 10^{-16}$
^{295}Rg/Au	raw platinum	0	$4.9 \cdot 10^{-14}$
^{295}X/raw Pt	raw platinum	0	$5.9 \cdot 10^{-16}$
^{298}Uuq/Pb	lead fluoride	0	$1.5 \cdot 10^{-14}$
^{310}X/raw Pt	raw platinum	0	$1.0 \cdot 10^{-15}$

Table 4.8: Overview on the results of the search for SHE. The upper limits were calculated as described in section 3.5 on a 1-σ confidence level.

4.7.2 Interpretation

The lack of events that could be attributed to SHE can have several reasons.
Firstly, the cause might be the r-process. It might simply be unable to produce SHE in sufficient amounts. Secondly, the half-lives of SHE could be so short that their abundance in the samples has dropped below our detection limits in the time since their synthesis until today. Another possible explanation lies in the chemistry of SHE. It cannot be excluded that instead of following their expected chemical homologues, geochemical processes might separate SHE from our sample materials.

Nonetheless, it was demonstrated, that the setup is able to distinguish any background events from possible SHE signals, which allows for very clean measurements. The established upper limits are orders of magnitude lower than those of comparable, earlier searches like for example those described in 1.4.4.
This project also serves to encourage future SHE searches with AMS. Although it is not easy to improve the upper limits in table 4.8 by orders of magnitude, because of the limited measuring times and currents, there are other possibilities to explore. Firstly, it would be interesting to extend the mass range further. There are other SHE candidates that are worth looking for, e.g. $^{304}120$. Extending the search to other sample materials would also be advantageous.

4.7.3 Outlook: Search for Strange Matter

Although it was not the goal of this research, the results also have implications on the topic of strange matter (SM).
SM is a hypothetical form of nuclear matter. Unlike normal nuclear matter which consists of protons and neutrons, which themselves consist of up- and down-quarks, strange matter consists of up- down- and strange-quarks in roughly equal proportion. Considering the Pauli exclusion principle, it is more favorable to fill quantum states with three types of quarks rather than two. Witten [75] and Bodmer [76] hypothesized that this effect could make SM stable at zero pressure (rather than at high pressure like inside neutron stars). If this is true, the ground state of nuclear matter could be SM. This would imply that normal matter decays to SM. However, the conversion of a nucleus of e.g. A=50 to strange matter would be of the 50th order in the weak interaction and thus very unlikely, even on a cosmological timescale. Normal matter can form stable nuclides ranging from A=1 (hydrogen) up to the hypothetical island of stability around A=300. Technically, there is another island of stability in a narrow region around A$\approx 10^{57}$ and Z$\approx 10^{56}$: neutron stars. The vast region of instability in between these extremes, spanning 55 orders of magnitude in mass, does not necessarily have to be empty. There might be several mass regions that could be inhabited by clumps of SM, so called strangelets. However, a strangelet of macroscopic size is usually referred to as a quark star [77]. Strangelets with a net positive charge could bind

electrons and appear atom-like with a lower Z/A value than normal nuclei.
For over 30 years, there have been suggestions that SM with any A might exist in nature. SM has also been postulated as a candidate for the dark matter content of the universe. Depending on the mass of the strangelets under consideration, several techniques for the search for SM in nature have been suggested. AMS can be used to search for strangelets with masses comparable to normal nuclei in nature. In a recent work, Han et al. conducted a search for strangelets in the mass range A=42 to A=70 [78] with AMS in a lunar sample. For details on other techniques, the reader is referred to an overview paper by De Rujula [79].

It is not excluded that strangelets are present in the raw platinum material we used for the search for SHE. In a sense, the masses A=292-295, and 310 were not only scanned for SHE, but also for strangelets with the same masses. Since this was not the primary goal of this project, the following does not present a complete analysis, but rather serves to demonstrate that the present setup can also be used for the search for SM in nature. This is done by estimating upper limits for the abundance of the two strangelets: ^{295}Fe (Z=26) and ^{295}Zr (Z=40), with m = 295.2 u each. The following points must be considered:

Masses Strangelets do not have a restriction to form integer mass numbers A because they do not consist of protons and neutrons. Thus, strangelets with e.g. m = 292.2 u, which is one of the masses we scanned, could exist.

Chemical behavior The chemical behavior of strangelets is almost unpredictable. Depending on the nuclear charge Z of the strangelet, the chemistry might resemble that of known elements. Similarly the yield of negative ion formation in the sputter ion source should be comparable to that of the normal element with the same nuclear charge.

Stripping yields Strangelets have a lower Z/A ratio than normal nuclei. Since the choice of charge states in the experiment was optimized for high stripping yields for SHE, the respective stripping yields for strangelets with low Z are not as high as those for SHE. To get an estimate for the stripping yields, they were calculated using the formulae from Shima et al. [80]. Since the charge state 10+ was chosen for the search

for SHE with A=295, the strangelets' stripping yields for the charge state 10+ must be calculated and we get an estimated yield of 0.01 % for ^{295}Fe and 0.3 % for ^{295}Zr (including a 50% error).

Without taking the chemical behaviour of ^{295}Fe and ^{295}Zr in the ion source into account, the following upper limits are obtained:

strangelet	Z	mass [u]	sample material	events	upper limit
^{295}Fe	26	295.2	raw platinum	0	$8.9 \cdot 10^{-13}$
^{295}Zr	40	295.2	raw platinum	0	$3.0 \cdot 10^{-14}$

Table 4.9: Example for the calculated upper limits for two strangelets on a 1-σ confidence level.

It should be emphasized again, that this does not represent a complete analysis of the implications of the experiment on the search for SM, because it was not the topic of this thesis. However, the calculations presented in table 4.9 show that the setup is also suited for a sensitive search for SM in nature. In an experiment that is exclusively dedicated to SM, it would be advantageous to choose lower charge states to get higher stripping yields.

List of Figures

List of Tables

Bibliography

[1] M. Asplund, N. Grevesse, and A.J. Sauval et al. The solar chemical composition. *Nuclear Physics A*, 777:1–4, 2006.

[2] E.M. Burbridge, G.R. Burbridge, W.A. Fowler, and F. Hoyle. Synthesis of the Elements in Stars. *Reviews of Modern Physics*, 29:547–650, 1957.

[3] A.G.W. Cameron. *Chalk River Report CRL*, 41, 1957.

[4] H. Grawe, K. Langanke, and G. Martinez-Pinedo. Nuclear Structure and Astrophysics. *Reports on Progress in Physics*, 70:1525–1582, 2007.

[5] J.M. Pearson, R.C. Nayak, and S. Goriely. Nuclear mass formula with Bogolyubov-enhanced shell-quenching: application to r-process. *Physics Letters B*, 387:455–459, 1996.

[6] K.L. Kratz. Nuclear Physics Issues of r-Process Nucleosynthesis. *AIP Conference Proceedings*, 819:409, 2006.

[7] S. Wanajo et al. The r-Process in Supernova Explosions from the Collapse of O-Ne-Mg Cores. *Astrophysical Journal*, 593:968–979, 2003.

[8] H. Ning et al. r-Process Nucleosynthesis in shocked Surface Layers of O-Ne-Mg Cores. *Astrophysical Journal*, 667:159–162, 2007.

[9] R. Surman at al. r-Process Nucleosynthesis in hot Accretion Disk Flows from Black Hole-Neutron Star Mergers. *Astrophysical Journal*, 679:117–120, 2008.

[10] V.S. Imshennik. Supernova 1987A and formation of rotating neutron stars. *Astronomy Letters*, 18:194, 1992.

[11] S. Rosswog et al. Mass ejection in neutron star mergers. *Astronomy and Astrophysics*, 341:499, 1999.

[12] C. Freiburghaus at al. r-Process in Neutron Star Mergers. *Astrophysical Journal*, 525:121–124, 1999.

[13] S. Wanajo, T. Kajino, G.J. Mathews, and K. Otsuki. The r-Process in Neutrino-driven Winds from Nascent, "Compact" Neutron Stars of Core-Collapse Supernovae. *Astrophysical Journal*, 554:578, 2001.

[14] H.J. Krappe, J.R. Nix, and A.J. Sierk. Unified nuclear potential for heavy-ion elastic scattering, fusion, fission, and ground-state masses and deformations. *Physical Review C*, 20:992, 1979.

[15] W.D. Myers and W.J. Swiatecki. Nuclear masses and deformations. *Nuclear Physics*, 81:1, 1966.

[16] E.O. Fiset and J.R. Nix. Calculation of Half-Lives for Superheavy Nuclei. *Nuclear Physics A*, 193:647, 1972.

[17] U. Mosel and W. Greiner. On the Stability of Superheavy Nuclei against Fission. *Zeitschrift für Physik*, 222:261, 1969.

[18] R. Smolanczuk. Properties of the hypothetical spherical Superheavy Nuclei. *Physical Review C*, 56:812, 1999.

[19] R.K. Gupta et al. Island of stability for superheavy elements and the dynamical cluster-decay model for fusion evaporation residue cross sections: ^{48}Ca+^{238}U$\rightarrow^{286}$112* as an example. *Journal of Physics G: Nuclear and Particle Physics*, 36:115105, 2009.

[20] M. Bender, W. Nazarewicz, and P.G. Reinhard. Shell stabilization of super- and hyperheavy nuclei without magic gaps. *Physics Letters B*, 515:42–48, 2001.

[21] G.T. Seaborg and W.D. Loveland. *The Elements beyond Uranium*. Wiley (New York), 2000.

[22] P. Armbruster. On the Production of Heavy Elements by Cold Fusion: The Elements 106 to 109. *Annual Review of Nuclear and Particle Science*, 35:135, 1985.

[23] G. Münzenberg. Recent advances in the discovery of transuranium elements. *Reports on Progress in Physics*, 51:57, 1988.

[24] S. Hofmann and G. Münzenberg. The discovery of the heaviest elements. *Reviews of Modern Physics*, 72:733, 2000.

[25] K. Morita, K. Morimoto, and D. Kaji et al. Experiment on the Synthesis of Element 113 in the Reaction ^{209}Bi(^{70}Zn, n)^{278}113. *Journal of Physics Society of Japan*, 73:2593–2596, 2004.

[26] Y. Oganessian et al. Synthesis of Superheavy Elements with ^{48}Ca beams. *Nuclear Physics A*, 682:108–113, 2001.

[27] Y.T. Oganessian. Experiments on the synthesis of element 115 in the reaction 243Am(48Ca,xn)291-115. *Physical Review C*, 69:021601, 2004.

[28] IUPAC Commission on Nomenclature of Inorganic Chemistry. Names and Symbols of Transfermium Elements. *Pure and Applied Chemistry*, 69:277, 1997.

[29] I. Zvara et al. Chemical Properties of Element 104. *JINR*, D:2710, 1966.

[30] A. Ghiorso et al. Positive Identification of two Alpha-Particle-emitting Isotopes of Element 104. *JINR*, D:2710, 1969.

[31] G.N. Flerov at al. Experiments on Search for alpha-radioactive Isotopes of Element 105. *JINR*, P7:3808, 1968.

[32] A. Ghiorso, M. Nurmia, K. Eskola, J. Harris, and P. Eskola. Observation of one correlated alpha-decay in the reaction 58Fe on 209Bi to 267109. *Physical Review Letters*, 24:1498–1503, 1970.

[33] K.E. Gregorich. First confirmation of the discovery of element 106. *Physical Review Letters*, 72:1423, 1994.

[34] G. Münzenberg. Identification of element 107 by α correlation chains. *Zeitschrift für Physik A: Atoms and Nuclei*, 300:107, 1981.

[35] G. Münzenberg. The identification of element 108. *Zeitschrift für Physik A: Atoms and Nuclei*, 317:235, 1984.

[36] G. Münzenberg. Observation of one correlated alpha-decay in the reaction 58Fe on 209Bi to 267109. *Zeitschrift für Physik A: Atoms and Nuclei*, 309:89, 1982.

[37] S. Hofmann. Production and Decay of ^{269}110. *Zeitschrift für Physik A: Hadrons and Nuclei*, 350:277, 1995.

[38] S. Hofmann et al. The new Element 111. *Zeitschrift für Physik A: Hadrons and Nuclei*, 350:281, 1995.

[39] Y.T. Oganessian. Synthesis of superheavy nuclei in the 48Ca+244Pu reaction: 288114. *Physical Review C*, 62:041604, 2000.

[40] Y.T. Oganessian. Observation of the decay of 292-116. *Physical Review C*, 62:011301, 2000.

[41] Y.T. Oganessian. Synthesis of a new element with atomic number Z=117. *Physical Review Letters*, 104:142502, 2010.

[42] Y.T. Oganessian. Synthesis of the isotopes of elements 118 and 116 in the 249Cf and 245Cm+48Ca reactions. *Physical Review C*, 74(4):044602, 2008.

[43] L. Donadille et al. Fission dynamics for capture reactions in 58,64Ni + 208Pb systems: New results in terms of thermal energy and neutron multiplicity correlated distributions. *Nuclear Physics A*, 656:259, 1999.

[44] G.M. Ter-Akopyan at al. JINR Dubna Report. 13:5391, 1970.

[45] R.L. Macklin et al. Neutron multiplicity counter. *Nuclear Instruments and Methods*, 102:181, 1972.

[46] D.A. Testov et al. Applications of ^{3}He Neutron Detectors. *Physics of Atomic Nuclei*, 72(1):1–5, 2009.

[47] P.B. Price et al. Search for Spontaneously Fissioning Elements in Nature. *Physical Review C*, 1:1819, 1970.

[48] U. Haack. Suche nach überschweren Transuranelementen. *Naturwissenschaften*, 60:65, 1973.

[49] A. Marinov et al. Evidence for a long-lived superheavy nucleus with atomic mass number A = 292 and atomic number Z = 122 in natural Th. arXiv:0804.3869v1, 2008.

[50] F. Deringer et al. Search for superheavy isotope with A=292 and neutron deficient Th isotopes in natural thorianite. Poster presented at AMS 11 - Rome, 2008.

[51] A.Z. Schwarzschild, P. Thieberger, and J.B. Cumming. . *Bulletin of the American Physical Society*, 22:94, 1977.

[52] W. Stephens, J. Klein, and R. Zurmühle. Search for naturally occuring superheavy element Z=110, A=294. *Physical Review C*, 21:4, 1980.

[53] D.E. Nelson et al. Carbon-14: direct detection at natural concentrations. *Science*, 198:507, 1977.

[54] C.L. Bennett et al. Radiocarbon dating usinc electrostatic accelerators: negative ions provide the key. *Science*, 198:508, 1977.

[55] R. Middleton. A very high intensity negative ion source. *Nuclear Instruments and Methods in Physics Research A*, 214:139–150, 1983.

[56] A. Urban. Beschleunigermassenspektrometrie mit ^{41}Ca. Diplomarbeit, Technische Universität München, 1986.

[57] G. Rugel et al. A Modified Negative Ion Sputter Source for AMS and its Efficiency for Plutonium. *Jahresber. des Beschleunigerlab. der Univ. und der TU München*, 2008.

[58] G. Korschinek, J. Sellmair, and A. Urban. A study of different ion sources for use in the ^{205}Pb experiment. *Nuclear Instruments and Methods in Physics Research A*, 271:328–331, 1988.

[59] C. Wallner. Beschleunigermassenspektrometrie mit Supernova-erzeugten Aktiniden. Dissertation, Technische Universität München, 2002.

[60] K. Knie. Beschleunigermassenspektrometrie mit Isobarenseparation in einem dedizierten gasgefüllten Magneten. Dissertation, Technische Universität München, 1996.

[61] D. Sailer. persönliche Mitteilung, 2010. Technische Universität München.

[62] J.F. Ziegler, J.B. Biersack, and U. Littmark. The Stopping and Range of Ions in Solids. *Pergamon Press*, 1, 1985.

[63] Impala Platinum. P.O. Box 5683, Rustenburg 0300, South Africa.

[64] http://www.implats.co.za/b/impala.asp. 05/05/2010.

[65] W. Carli. persönliche Mitteilung, 2010. Ludwig-Maximilians Universität München.

[66] G.J. Feldmann and R.D. Cousins. A Unified Approach to the Classical Statistical Analysis of Small Signals. *Physical Review D*, 57(7):3873–3889, 1998.

[67] R.O. Sayer. Oak Ridge National Laboratory. *Tennessee 37830*, 1977.

[68] A.G. Demin et al. Experiments on the synthesis of element 108. *JINR*, P7:84, 1984.

[69] Ch.E. Düllmann et al. Chemical investigation of hassium (element 108). *Nature*, 418:859–862, 2002.

[70] M. Schädel and A. Türler. Ein Platz für Schwergewichte. *Physik Journal*, 8:30–35, 2009.

[71] Alfa Aeser GmbH & Co KG. A Johnson Matthey Company, Postfach 110765, 76057 Karlsruhe.

[72] O.L. Kellner, C.W. Nestor Jr., and T.A. Carlson. Predicted properties of the superheavy elements, II. element 111, eka-gold. *Journal of Physical Chemistry*, 77:1806–1809, 1973.

[73] H.W. Gäggeler and A. Türler. *The Chemistry of Superheavy Elements.* Kluwer Academic Publisher, 2003.

[74] M. Jacoby. As-yet-unsynthesized superheavy atom should form a stable diatomic molecule with fluorine. *Chemical and Engineering News*, 84(10):19, 2006.

[75] E. Witten. Cosmic Separation of Phases. *Physical Review D*, 30:272, 1984.

[76] A. Bodmer. Collapsed Nuclei. *Physical Review D*, 4:1601, 1971.

[77] F. Weber. Strange Quark Matter and Compact Stars. *Progress in Particle and Nuclear Physics*, 54:193–288, 2005.

[78] K. Han et al. Search for stable strange quark matter in lunar soil. *Physical Review Letters*, 103:092302, 2009.

[79] A. De Rujula. Aborigines of the nuclear desert. *Nuclear Physics A*, 434:605–626, 1985.

[80] K. Shima, T. Ishiara, and T. Mikumo. Empirical formula for the average equilibrium charge-state of heavy ions behing various foils. *Nuclear Instruments and Methods*, 200:605–608, 1982.

Upon the completion of the thesis I would like to make use of the opportunity to thank several people for their support and contributions. My thanks go to:

- Prof. Dr. Shawn Bishop, for providing me with the opportunity to complete this project at the chair E12.
- Dr. Georg Rugel, for all the time he put in to answer all my questions, to familiarize me with the AMS system, and for lots of night shifts during beamtimes.
- Dr. Gunther Korschinek, for his support for the project and a lot of help modifying the beamline.
- Dr. Thomas Faestermann, for a lot of good ideas for the project and solving problems with the electronics and theory.
- Dr. Iris Dillmann, for introducing me to the GAMS group in the first place and for many interesting discussions on astrophysics.
- Ursel Heim, for sharing the office with me and contributing to a wonderful working atmosphere.
- the operators, for all the help during the beamtimes.
- the MLL workshop, for helping with the reconstruction of the beamline.
- Norbert Gärtner and Walter Carli for hooking up the new Wien-filter.
- Prof. Dr. Michael Paul, for organizing the new Wien-filter.
- Rudi Lutter, for helping with computer problems.
- Dominik Sailer, for the new Lensodel foils.
- Pankaj Baghel, for preparing the ion sources and helping with the beamline.
- Stefan Waldherr, for providing LaTeX support.
- my mother Bärbel, my late father Kurt, and my uncle Klaus, for supporting me all my life.